

Mechanisms and Causes of Amplitude Modulation (AM) and Other Amplitude Modulation (OAM) of Aeroacoustic Wind Turbine Noise

DTU Vindenergi
Report 2013

Helge Aagaard Madsen

Andreas Fischer

Knud Abildgaard Kragh

DTU Wind Energy I-0095 (EN)

ISBN: xxx-xx-xxxxx-xx-x

August 2013

DTU Vindenergi
Institut for Vindenergi



Authors: H. Aa. Madsen, A. Fischer and K. A. Kragh
Title: Mechanisms and Causes of Amplitude Modulation (AM) and Other Amplitude Modulation (OAM) of Aeroacoustic Wind Turbine Noise inflow measurements

August 2013

Pages:46

Tables: 0

References: 13

Technical University of Denmark

www.vindenergi.dtu.dk

Contents

1	WP1: Compilation of Results	8
1.1	Objectives	8
1.2	Observed wind shear	8
1.3	Correlation of wind shear to AoA	9
1.4	Modelling rotor aerodynamics with wind shear inflow	14
2	WP2: Aero-acoustic Modelling	17
2.1	HAWC2 computations on NREL 5MW turbine	17
2.2	HAWC2 computations on modified NREL 5MW turbine	19
2.3	Surface pressure characteristics of NM80 2.3MW wind turbine (DANAERO)	20
2.4	Aeroacoustic modelling	27
3	WP3: Mitigation Strategies	32
3.1	Collective Pitch Control	32
3.2	Individual Pitch Control	32
3.3	Yaw Control	34
4	WP4: Effect of Stall on Noise Emission	37
4.1	Airfoil aerodynamics	37
4.2	Far field Sound and Surface Pressure for High AoAs	37
4.3	Far field Sound Modelling for high AoA in Pre Stall	40
4.4	Conclusions	40
A	Turbines used in the investigation and influence of turbine size	43
B	Difference between angle of attack AoA and inflow angle IA	45

Executive summary

The work explores the mechanisms and causes of amplitude modulation (AM) of aeroacoustic noise from wind turbine rotors and specially the occurrence of lower frequency amplitude modulation identified by RenewableUK at different sites and denoted "other amplitude modulation" (OAM). The work has been organised in four work packages (WP) according to: "Description of Contract Work for RenewableUK on Mechanisms of AM and OAM", DTU Wind August 15, 2012 and Revised January 28, 2013.

WP1: Compilation of Results

The objectives with this WP are:

- Illustrate from literature what variations of wind shear have been measured.
- Show the correlation of wind shear to variations in angle of attack (AoA).
- Show modelling capabilities of influence of wind shear on rotor aerodynamics.

A characterisation of measured wind shear from 40-160m height over one year at the Høvsøre wind turbine test site shows that the strongest wind shear with a variation in wind speed of about 4.5 m/s from 40-160m occurs 2.7% of the time. The experimental proof of the link between wind shear and angle of attack variations (AoA) comes from the DANAERO experiment carried out from 2009 to 2010 in Denmark. As explained in Appendix A, AoA cannot be measured directly on a rotor but instead a local inflow angle (IA) to a blade section of the blade can be measured and, in the present case, at radius 36m on a 52m blade. In figure 8 it is shown how the IA as a function of blade azimuth position varies during a period of 7 hours where the wind shear develops from an extreme level during night conditions to almost no shear at 11.00am. This data is further processed so that the range of IA variations over one rev is shown as a function of the slope of the linear wind shear approximation, figure 12. To show the link between wind shear and AoA, simulations were run for the same wind shear slopes and the computed AoA were converted to IA, which can then be compared with the measured IA curve, figure 12.

The overall conclusion from the measurements and the computations is that there is experimental evidence of AoA variations of at least 4° - 5° for extreme wind shear, based on the data in figure 12.

Finally, some results from using different computational models of a wind turbine operating in strong shear conditions are presented, illustrating, for example, how the low speed flow on the ground can move up into higher levels a few diameters down in the wake due to wake rotation. This could cause quite different AoA variations on a downwind turbine operating in this wake.

WP2: Aero-acoustic Modelling

There are three parts in WP2. In the first part, (sections 2.1 and 2.2) a number of simulations results are presented to illustrate how different wind shear and turbulence conditions in the inflow to the rotor cause AoA variations. The simulations are carried out on a 5MW reference wind turbine; a turbine defined within the research community, with all design data freely accessible. Further description of the turbine can be found in Appendix A. A range of AoA variations are depicted in figure 17 for different wind shears and turbulence intensities. Overall there is an almost constant level from 7-10m/s wind speed and both the mean and the

amplitude increase slightly from 10-12m/s before the mean then decreases when the turbine reaches rated power. It can be seen that turbulence increases the range compared with only shear conditions.

As shown on the left part of figure 21, the turbine operates on the lift coefficient curve well below beginning stall. However, if the planform is modified as shown in figure 18 to a more slender blade design, as has been the tendency in blade design for some years, the operating point moves upward as seen on the upper curve in figure 20. Now the variation around the mean AoA level is seen to reach the non-linear part of the lift curve slope due to initial trailing edge separation.

The second part of WP2 is an analysis of high frequency surface pressure measurements on a NM80 turbine carried out within the DANAERO project. The present analysis is focused on time series where the turbine was forced to approach stall by pitching the blade to -5° . and running the turbine at constant speed but at a reduced level compared with rated speed. Further there was a considerable shear in the inflow. The signal from a microphone close to the trailing edge was analysed representing the source of trailing edge noise. During a period AoA variations were up to a range of 4.5° . with the maximum AoA reaching 13° , figure 28. During this period an extreme level of AM was seen with a range over rotor rev of 14dB in the frequency range below 200 Hz, figure 29 and 30.

The third part of WP2 contains simulation results of turbulent inflow (TI) noise and trailing edge noise (TE) for different inflow conditions to the turbine. The directivity of TE noise is at a maximum for the blade in the 3 o'clock position as seen in figure 35, whereas the peak inflow angle for a strong shear is in the 12 o'clock position, figure 34. For a listener 70m downstream, this combination of directivity and AoA leads to a peak sound from the rotor at around a 1-2 o'clock position, figure 33. For the TI noise the peak value for the same listener position is at the 6 o'clock position, figure 36.

WP3: Mitigation strategies

Three mitigation strategies are investigated; 1) collective pitch control for decreasing the mean AoA and in this way move the operating point on the lift curve away from stall; 2) individual pitch control (IPC) in order to reduce the AoA variations and 3) yaw control also to reduce AoA variations.

The use of the collective pitch system to reduce the mean AoA is a well-known procedure for reduction of broadband noise from a wind turbine. However, it may also be an efficient method to reduce AM of noise if the rotor is operating close to stall. A demonstration of reducing the mean AoA is shown in figure 37 where the minimum pitch setting in the control has been increased from 0° up to 5° . However, in particular for mean pitch angles greater than 2° . the power loss increases significantly as shown in the right graph of figure 37.

Next the effect of applying IPC is demonstrated. In the present case it is a standard IPC that is set up to reduce the blade root bending moments. However, in most cases it will also reduce the AoA variations and in particular what is due to wind shear (see left graph in figure 38). When there is considerable turbulence in the inflow the effect of IPC is less promising (right graph in figure 38). The power loss by applying IPC is in general small and less than 1% as seen in figure 39.

Finally, the effect of operating the turbine at different yaw errors is simulated. For operation in wind shear it seems that a yaw error can be found as a function of wind speed which leads to an AoA variation that is less than running the turbine at zero yaw error, figure 41. A reduction of about three quarters of a degree. can be obtained. On the other hand; if the turbine is operating at a yaw error to the other side this can cause considerable AoA variations, figure 41.

WP4: Effect of Stall on Noise Emission

The study was carried out as an extension of a previous analysis of an existing data set measured by DTU Wind Energy in the Virginia Tech University wind tunnel in 2011. In particular the study was focused on analysis of data measured at high AoA in the wind tunnel to see the effect of stall on the airfoil. The experimental set-up comprised two airfoil sections with around 60 surface pressure microphones each, plus an acoustic array outside the tunnel. Also the surface pressure distribution on the blades was measured.

Due to limitations of the operational frequency range of the microphone array it did not provide data below 1000 Hz, figure 45, so the main conclusions have to be done on basis of the surface microphones. Considerable increases in the surface pressure spectra below 1000 Hz are seen when entering into stall, figure 46. The level increase is more than 10dB at a frequency of 200Hz when going from pre-stall to stall. A numerical model is applied to derive the far field sound based on the surface pressure measurements for AoA up to pre-stall . At a frequency of 200Hz the far field sound is modelled to increase with 2.8dB for just one degree increase in AoA.

1 WP1: Compilation of Results

1.1 Objectives

The objectives with this chapter are to:

- Illustrate from literature what variations of wind shear that have been measured
- Show the correlation of wind shear to variation in angle of attack (AoA) or inflow angle (IA)
- Show modelling capabilities of influence of wind shear on rotor aerodynamics and the influence on AoA variations

Deriving results on these subjects will constitute the basis for using numerical investigations in the next chapter to further investigate what the influence wind shear and turbulence in the inflow of a MW turbine has on AoA variations and to see if this can lead to initial trailing edge separation.

1.2 Observed wind shear

The information presented in this section is from a paper by Antoniou et al. [1] from 2007 where the wind shear characteristics measured over one year at the wind turbine test site at Høvsøre in Denmark have been presented.

Citation from paper:

”The Høvsøre test site is the National Danish Test Station for Large Wind Turbines, which is situated in the northwest of Denmark, close to the North Sea. The test site is flat, surrounded by grassland with no major obstacles and is situated a distance of 1.7 km from the west coast of Denmark. The prevailing wind direction is from the west. Figure 1 shows the site layout and the instruments used. The wind profiles have been produced combining the measurements from two met masts at the Høvsøre test site. The two met masts are the aviation light met mast, and the met mast to the right of the picture.”

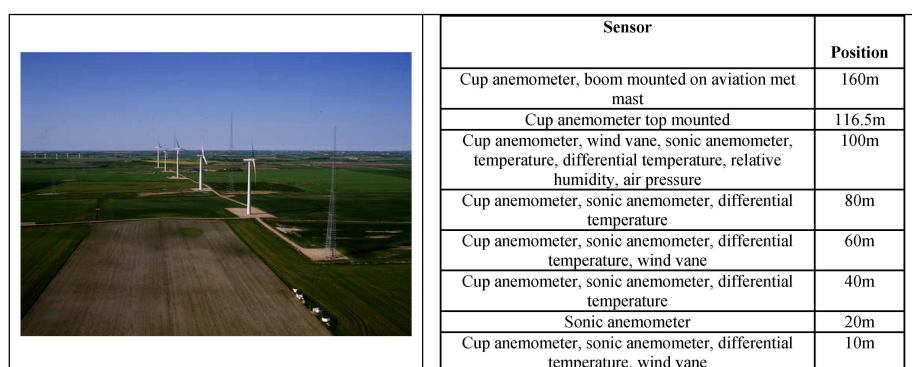


Figure 1. The test site and the heavily instrumented met tower along with a list of the available instruments.

The analysis was carried out using data from the cup wind speeds at 40m, 60m, 80m, 100m, 116m and 165m. An example of the wind speeds measured during one day in March 2007 is shown in figure 2. The wind shear is mainly determined by

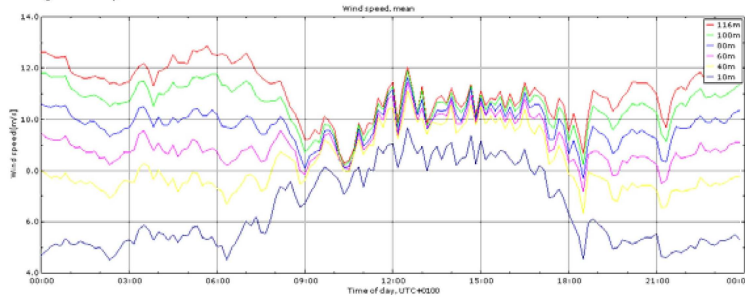


Figure 2. The wind profile during the 29th of March, 2007.

the atmospheric stability. At night the atmosphere is stable and we see a large wind shear but during daytime when the sun heats up the atmospheric boundary layer the atmosphere becomes unstable and the wind shear almost disappears.

For the analysis procedure of the data we cite from the paper:

”the wind profiles from 6m/s to 8m/s for the height of 80m and for one year period were chosen. Within this period, 2340 profiles were found from the easterly directions between 60° and 120°, which were binned and categorised according to their shape into 173 profiles, non-equally weighted, figure 3. Subsequently all mean profiles were normalised so that the wind speed at 80m became equal to 7m/s, $U_{80} = 7\text{m/s}$, using the ratio $Ri = 7/U_{80}$, where i is the profile number, see figure 3(b).”

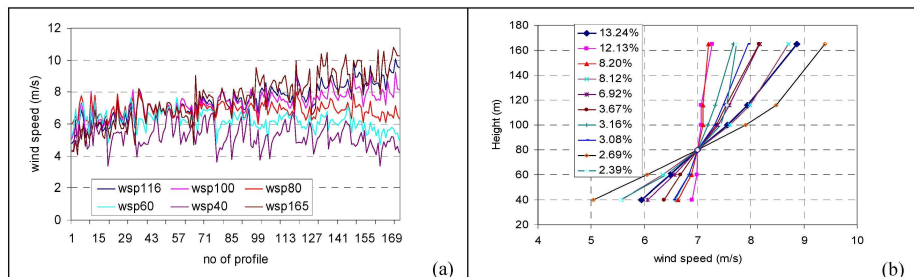


Figure 3. (a): The classified 173 easterly wind profiles, (b): the 10 most common normalised profiles and their percentage of occurrence.

For the strongest wind shear occurring 2.69% of the time, the variation in wind speed from 40m height to 160m height is close to 4.5m/s. The wind shear with a variation of 3m/s occurs more than 13% of the time. In summary wind shear with a variation from 3m/s to 4.5m/s over 120m heights can occur regularly.

1.3 Correlation of wind shear to AoA

Most of the information on this subject is from the paper of Madsen and Fischer [2] but results from new analysis of data are also included. In ref. [2] the results on measuring the inflow to the rotating blade of a Siemens 3.6MW turbine at the Høvsøre test site were presented. These measurements were part of the DANAERO MW experiment [3] carried out in the period from 2007 to 2010. The objective with this part of the project was to investigate experimentally the inflow to a MW turbine during different atmospheric conditions. The inflow measurements

were made with a five hole pitot tube¹ mounted at 36m radius on the rotor with a diameter of 123m (59% of the blade length), figure 4. These measurements were then correlated with wind speed measurements in a nearby meteorology mast instrumented with anemometers at heights position 10m, 40m, 60m, 80m, 100m and 116.5m and wind direction vanes at height position at 10m, 60m and 100m. Results

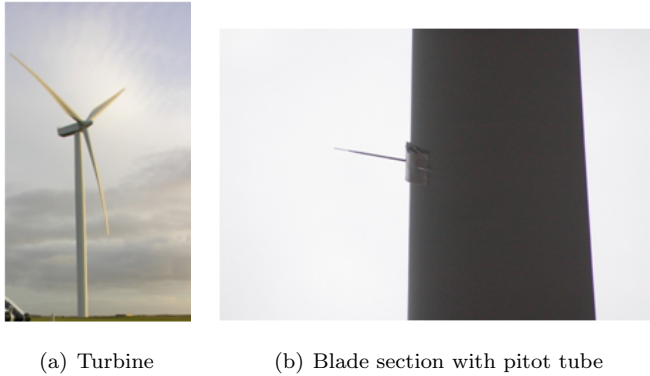


Figure 4. The five hole pitot tube mounted in radius 36 m on the blade in a distance of about 0.80 m in front of the leading edge of the blade.

from analysis of data during the day March 28 in 2007 are presented. That day was selected because it is a typical example of inflow conditions varying strongly from day to night with very stable atmospheric conditions during night time and thus strong wind shear, whereas during daytime the sun heats the atmospheric boundary layer creating a lot of mixing with the result that the wind shear almost disappears. In figure 5 the wind shear measured during one week in March 2007 is shown and the same daily pattern with strong shear during night and almost no shear during the day can be seen. The March 28 wind shear data are shown

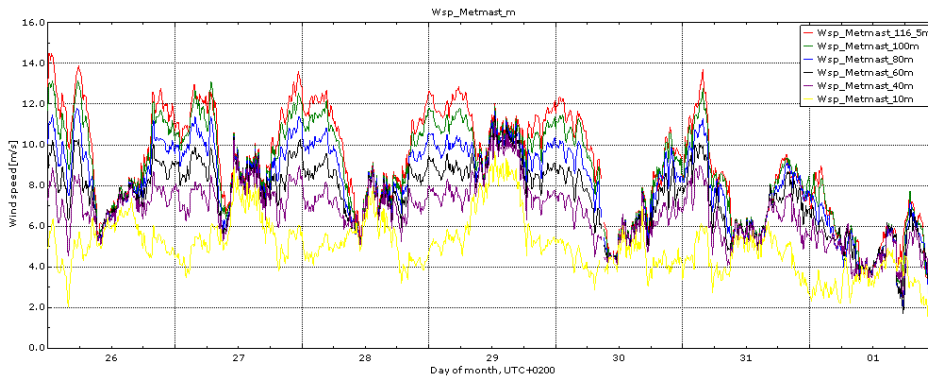


Figure 5. Measurements of wind shear at the Høvsøre test site during one week from March 26 to April 1st in 2007.

in more details in figure 6. The wind direction measured at three heights is also shown and a strong wind veer of 20° – 25° occurs during night time but during daytime it disappears completely.

The inflow to the rotating blade of the Siemens turbine was measured during the same period. The inflow angle IA to the blade measured with the pitot tube is shown in figure 7 as a function of azimuth and each curve was derived for a period of 10 min. by binning the instantaneous IA on azimuth position. It should be

¹A flow sensor that can measure the inflow velocity vector (two angles and the magnitude of the velocity vector) relative to the blade.

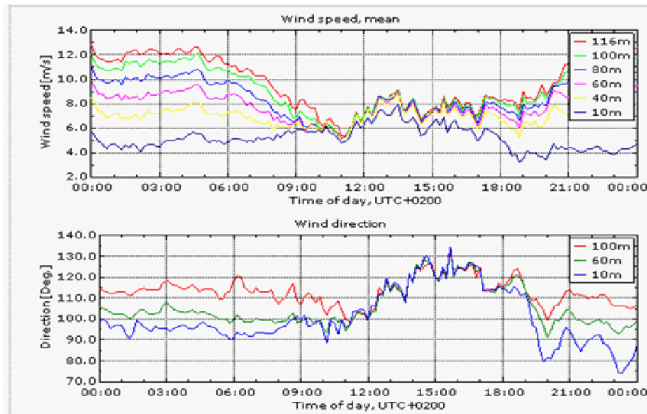


Figure 6. Variation of wind shear and wind veer during March 28, 2007 at the Høvsøre test site.

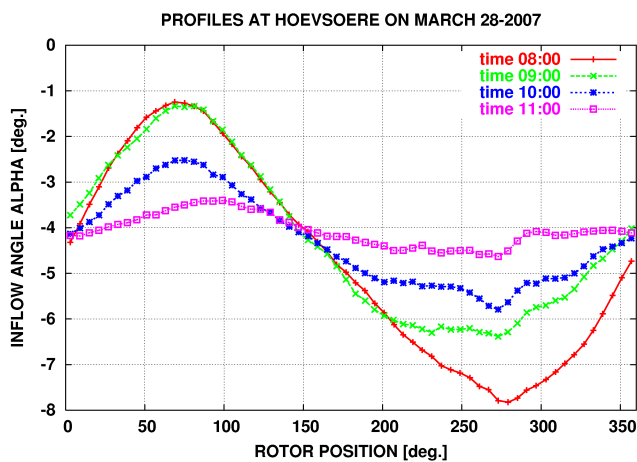


Figure 7. Inflow angle variations as a function of azimuth (10 min average) measured from 8 o'clock to 11 o'clock each hour on March 28, 2007. See the shear in inflow above. It should be noted that this is local inflow angles measured on the blade and not corrected for upwash.

noted that the IA is influenced by the local flow around the airfoil (upwash) and therefore not equal to AoA but typically showing bigger amplitudes. Further, it should be mentioned that the mean value of IA has not been calibrated.

Comparing now the four curves measured at each hour in the time interval from 8 to 11 o'clock in the morning it is seen that the amplitude over azimuth is reduced considerably. The blade top position is 90° , the blade bottom position is 270° . The biggest variation of IA is seen at 8 o'clock where it is about 9° with the maximum value reached $10^\circ - 20^\circ$ before the blade is in top position. It is also seen that the curve is quite smooth but with a small irregularity around 270° where the blade passes upstream of the tower. Comparing now with the curve measured at 9 o'clock it is seen that the reduction in amplitude only can be seen on the lower part of the rotor. Then the further reduction in amplitude during the next hour is seen over the whole rotor disc and finally at 11 o'clock the variation in IA is reduced to about 1° . Correlating the observed variations in IA with the development in wind shear shown in figures 5 and 6, the decrease in IA amplitude follows the decrease in wind shear.

Besides the data from reference [3] additional analyses of data from the night of

March 28 have been added to the previous IA data set and are shown in figure 8. The new data at 4 and 5 o'clock at night show even bigger amplitude with a

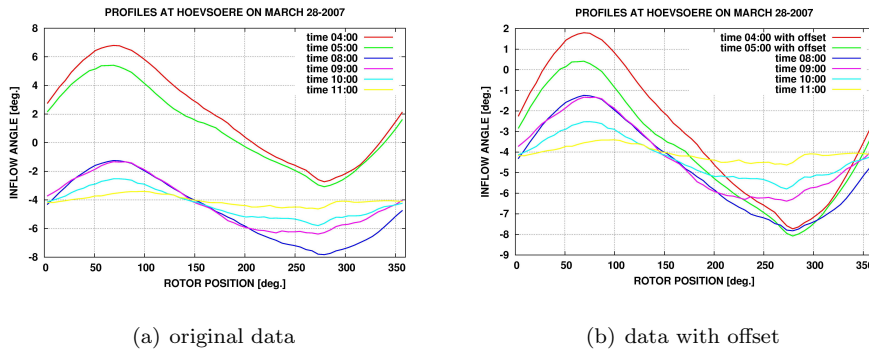


Figure 8. Extended data set on inflow measured during the night/morning of March 28, 2007.

maximum of $9^\circ - 10^\circ$. In the left figure the raw data is shown whereas in the graph to the right an offset of -5° has been added to better compare the amplitudes. The measured relative velocity profiles are shown for the same period in figure 9. In particular the profiles at 4 and 5 o'clock in the morning show a drop in relative

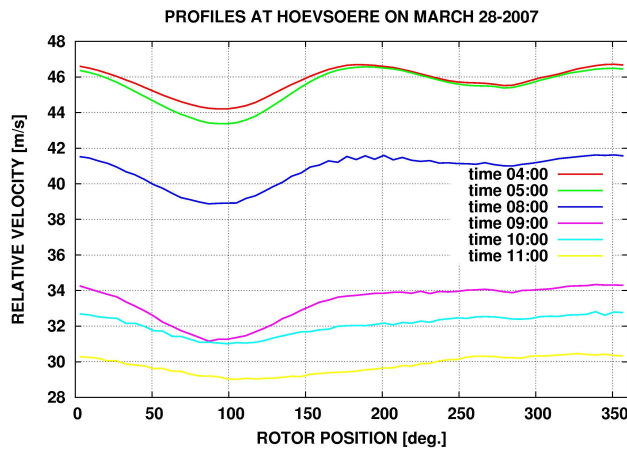


Figure 9. Measured relative velocity corresponding to the IA data in figure 8.

velocity at an azimuth of 90° and at 270° . This is probably caused by the wind veer which has most influence on the relative velocity and less on the IA. Based on the wind shear data in figure 6 the development of the wind shear profiles in the time from 4 to 11 o'clock on March 28 were derived and are shown in figure 10. To parameterize the profiles, the exponential wind shear law was tested but did not fit so well and it turned out that a linear wind shear approximation in the height range of the rotor worked better and is shown in figure 11. With this parameterization of the wind shear profiles we can now form the link to the IA variations for the rotor blades that was shown in figure 8. The correlation between wind shear and IA variations is shown in figure 11 and it is seen that it is quite non-linear. The causes for this are not clear. Now we would like to establish the link to AoA instead of IA because AoA can give us the link to the operational point on the airfoil lift curve and thus also investigate possible beginning stall. However, it is easier to convert simulated AoA to IA than correct measured IA to

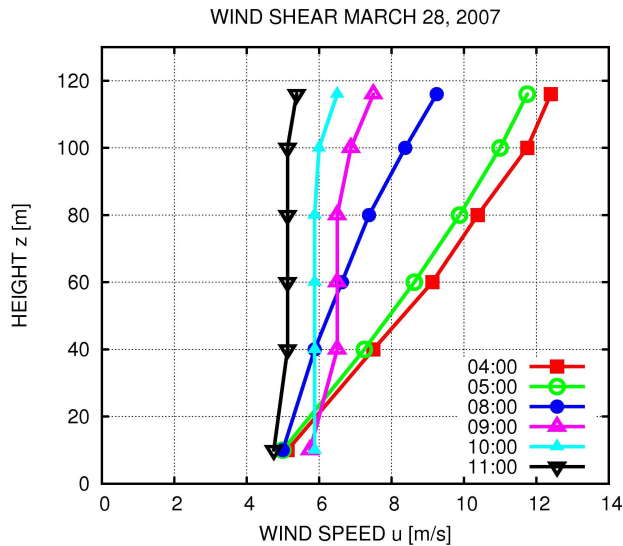


Figure 10. Wind shear profiles derived from the data in figure 6.

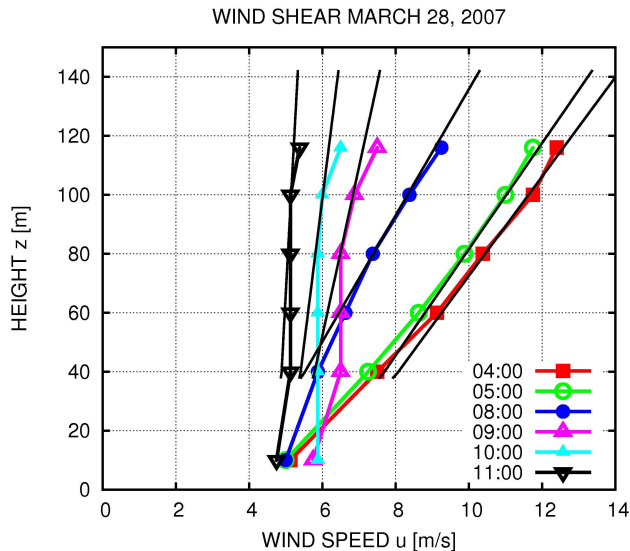


Figure 11. Wind shear profiles approximated with a linear shear variation.

AoA. The procedure chosen was therefore to take the approximated linear shear profiles and run a simulation with the aeroelastic code HAWC2² to simulate the corresponding AoA variations for these linear wind shear profiles. The AoA variations are the red curve in figure 12. Finally, the simulated AoA were corrected to simulated IA shown as the green curve in figure 12. Ideally, this curve should have coincided with the measured blue curve but deviations occur. This can be ascribed to different uncertainties: 1) the uncertainty in the conversion procedure from AoA to IA; 2) simulations were done for the wind shear profiles approximated with a linear wind shear variation and finally 3) the model uncertainty of

²HAWC2 is an aeroelastic code developed at DTU and can simulate the rotor aerodynamics and the aeroelastic response of a wind turbine for specified inflow such as wind shear and turbulence.

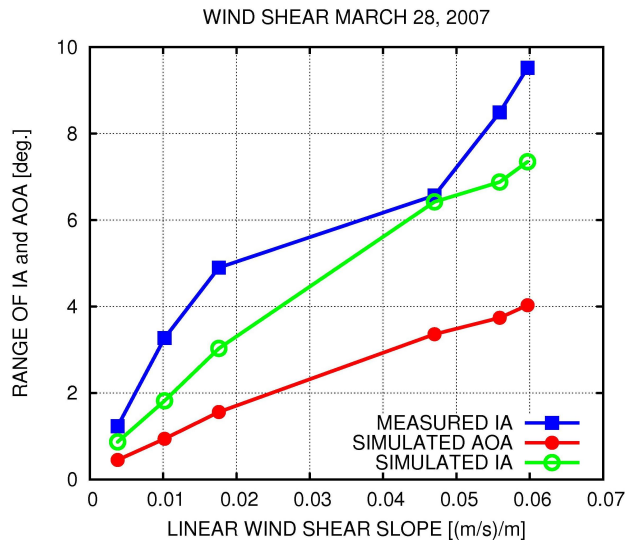


Figure 12. Wind shear profiles approximated with a linear shear variation.

HAWC2. However, we have established the relation between the wind shear and AoA variations and for the extreme wind shear conditions we can expect a range of AoA variation over one rotor revolution up to 4° and maybe 5°.

1.4 Modelling rotor aerodynamics with wind shear inflow

Wind shear in the inflow makes the rotor aerodynamics much more complicated compared with uniform inflow and therefore this has been an important research subject during recent years e.g. within the EU funded project UpWind finished in 2011. The results presented in this section are mainly from a paper by Madsen et al. [4] that contains the major results from the work on rotor aerodynamics in combination with wind shear in the inflow. In particular the aim here is to prove that the influence of wind shear can be modelled with reasonable accuracy using the aeroelastic model HAWC2 which later in this study will be used for a more systematic investigation on how wind shear affects AoA variations and whether this can lead to initial trailing edge stall.

Advanced models such as computational fluid dynamics (CFD) codes and vortex codes were in reference [4] used to gain insight into the rotor and wake flow in combination with strong wind shear in inflow. Contours of axial velocities at two downstream positions 1D and 3D from a CFD rotor computation with a wind shear exponent of 0.5 are shown in figure 13. The major influence of the rotor is the reduction in axial velocity but also some interaction with the ground is seen in the form of an acceleration just below the rotor. Another major characteristic is that the swirl of the flow in the wake causes the low velocities at the bottom part of the rotor to slowly turn anti-clockwise in the wake and at 3D downstream it covers almost one side of the wake from ground to top. This would give an even more complex inflow situation for a turbine positioned in the wake of the first turbine.

The advanced models (CFD and vortex codes) were, in the UpWind project, used to investigate the uncertainty of the computations from the simpler models, typically the aeroelastic codes used for time simulations of aeroelastic response in industry as well as by research institutes. The very simple reason to use the simpler

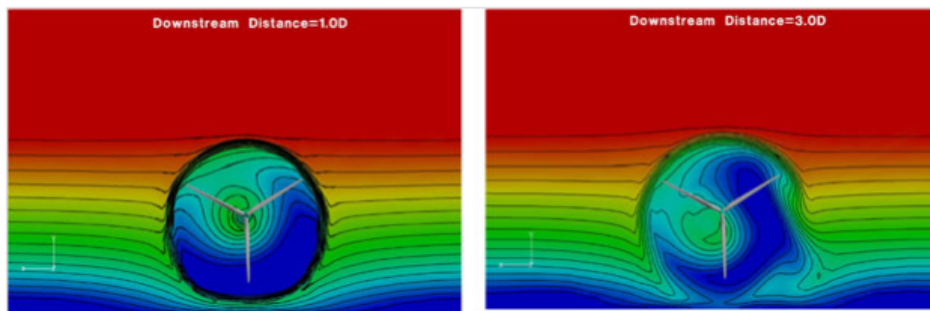


Figure 13. Computed flow field around a 126m diameter rotor operating in extreme wind shear with an exponent of 0.5. Computations are from computations with the 3D CFD code EllipSys3D and the axial wind speed contours are shown at a position of 1D and 3D downstream the turbine.

models is that they are an order of magnitudes faster than the CFD models. The comparisons carried out in the UpWind project showed that during uniform inflow all the models gave very similar results with power and thrust within a range of 1%. However, for strong shear in the inflow the deviations between the codes become bigger as shown in figure 14 where the induction along the blade is shown for four blade positions; blade pointing upwards is pos. 0° . The advanced

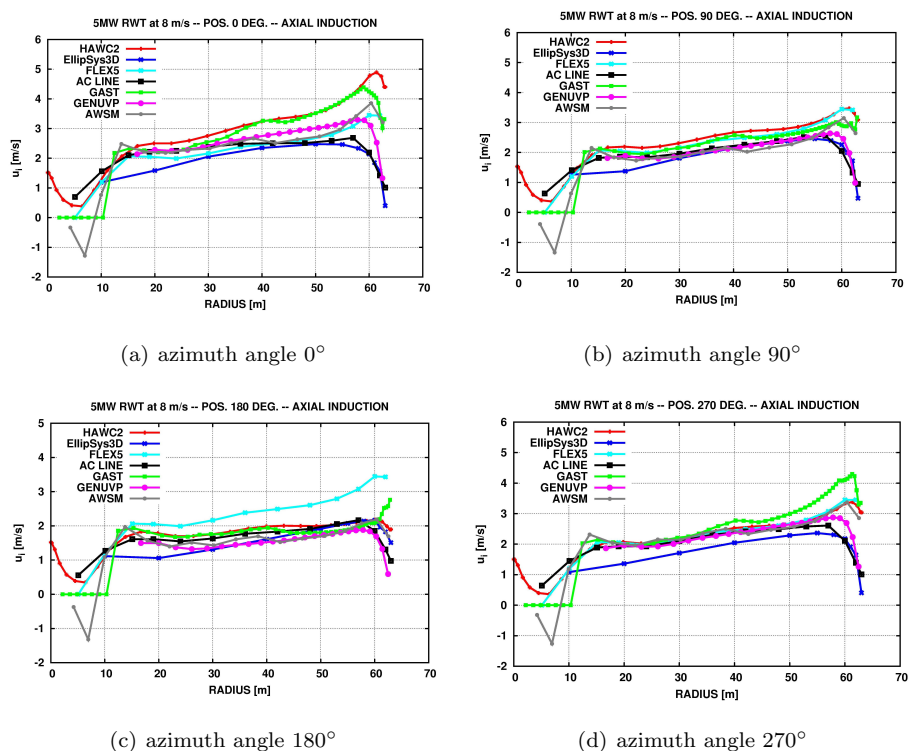


Figure 14. Computed induction for the 5MW reference turbine with a 126m rotor using a number of different codes of different complexity.

model results in this figure are: the CFD codes EllipSys3D and ACL and the vortex codes GENUVP and AWSM. The other codes HAWC2, FLEX5 and GAST are the simpler engineering codes with the Blade Element Momentum BEM model for the induction. It is seen that in particular for the blade pointing upwards, the induction computed with the HAWC2 code and the GAST code seems to exceed the advanced model results. However, for the three other positions the results

are rather close. The influence of the observed deviation in induction is that the HAWC2 code might compute an AoA for the blade in top position that is slightly lower than the true value for the cases with strong wind shear in the inflow.

2 WP2: Aero-acoustic Modelling

2.1 HAWC2 computations on NREL 5MW turbine

The NREL 5MW reference turbine is a conceptual turbine developed by Jonkman [5]. All the details needed for aeroelastic modelling of this turbine are publicly available. The design is close to the REpower 5MW turbine, but there is also a significant difference to real turbines. The blades of the NREL 5MW turbine operate at comparatively low angles of attack. Hence there is a large margin to the stall angle and transient stall over one rotor rotation is therefore very unlikely. But this design leads to large chord lengths and heavy blades. Modern MW wind turbines have more slender blades and the airfoils operate at higher angles of attack.

We simulated different normal operation conditions. The inflow was either uniform or sheared according to a power law. The exponent of the power law was varied from 0.1 to 0.5 in steps of 0.1. Inflow turbulence is simulated with the Mann turbulence model [6]. We simulated with a turbulence intensity of 0.0 (no turbulence), 0.1 and 0.2. The wind speed was varied in steps as shown in figure 15. The typical behaviour of the turbine is presented for the case with uniform inflow

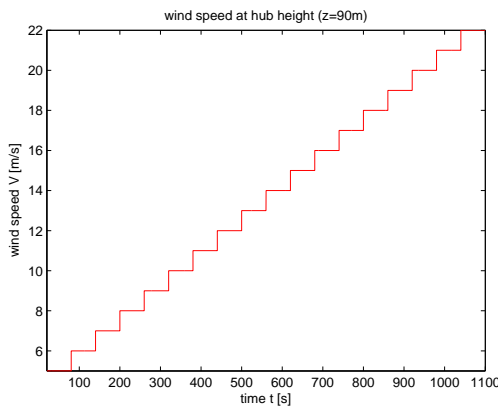
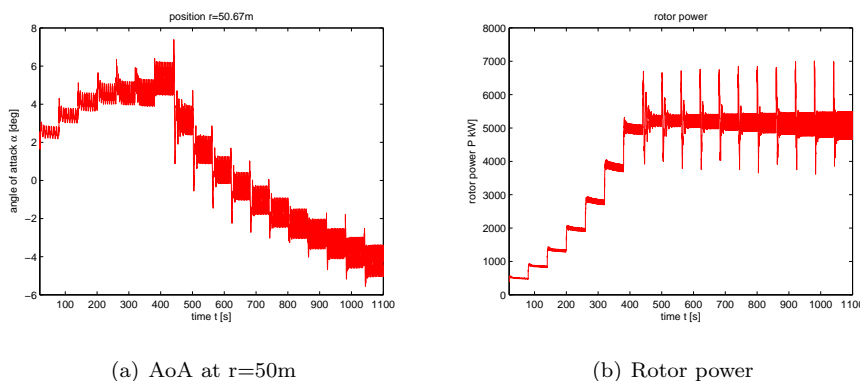


Figure 15. Wind speed at 90m (hub height) in the simulation without turbulence.

and no turbulence by means of the AoA at $r=50\text{m}$ and the rotor power, figure 16. The AoA at radial position $r=50\text{m}$ (79.4% of the total blade length) varies



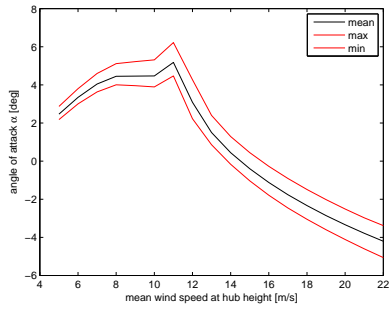
(a) AoA at $r=50\text{m}$

(b) Rotor power

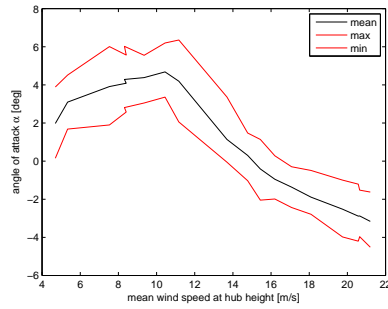
Figure 16. Simulation with uniform inflow and no turbulence.

periodically with the rotor rotation. The average value as well as the amplitude

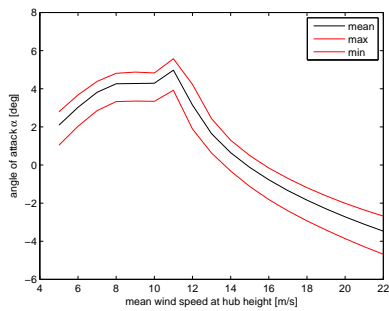
of the modulation grow with increasing wind speed. A maximum is reached for a wind speed of 11m/s when the turbine is close to rated power. When rated power is reached, the controller starts to pitch the blades and the AoA is decreased. The highest AoA obtained in the operational range is $\alpha = 6^\circ$. The airfoil sections at the outer part of the blade have maximum lift at $\alpha = 14^\circ$. The airfoil drag starts to increase more rapidly at AoA $\alpha = 10^\circ$. That means that flow separation at the rear part of the suction side is possible at this AoA. However, for this turbine it is very unlikely that transient stall occurs in uniform inflow with no turbulence. The impact of turbulence and wind shear is visualized in figure 17.



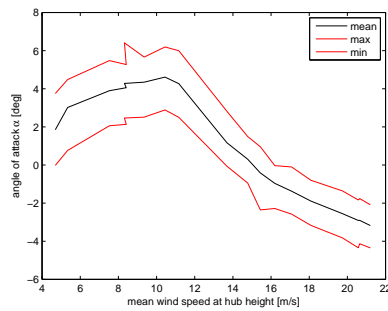
(a) Uniform Inflow, No Turbulence



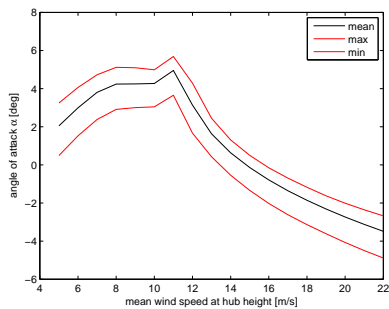
(b) Uniform Inflow, $T_i=0.2$



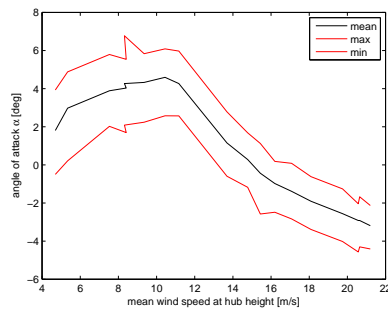
(c) Sheared Inflow $\text{exp}=0.3$, No Turbulence



(d) Sheared Inflow $\text{exp}=0.3$, $T_i=0.2$



(e) Sheared Inflow $\text{exp}=0.5$, No Turbulence



(f) Sheared Inflow $\text{exp}=0.5$, $T_i=0.2$

Figure 17. Amplitude and mean values of the AoA as function of the wind speed.

The figures were generated by extracting the mean value and the maximum and minimum of the AoA for each 60 second time segment within a step of the wind speed. The first 15 sec after stepping the wind speed were discarded to avoid the unrealistic peaks. Wind shear has an influence on the amplitude of the AoA only at low wind speeds. Turbulence has a stronger influence on the amplitude and the influence is noticeable in the whole wind speed range. The mean value of the AoA is not much effected by shear or turbulence. In no case did the highest AoA obtained in operation exceed $\alpha = 6^\circ$ by very much. Transient stall will not occur on such a blade.

2.2 HAWC2 computations on modified NREL 5MW turbine

The design of the NREL 5MW reference turbine is very conservative. In a more realistic design the airfoils are operated at higher AoAs to achieve a higher lift. This leads to slender blades, because the chord length of the airfoils can be reduced. It is very important to reduce the weight of the blades of MW wind turbines. Therefore the slender blade is a more realistic setup.

We redesigned the blade of the reference turbine by decreasing the chord length and twisting the blade to higher AoAs in compensation for the loss in lift. The new chord distribution compared to the old one is displayed in figure 18. The lift

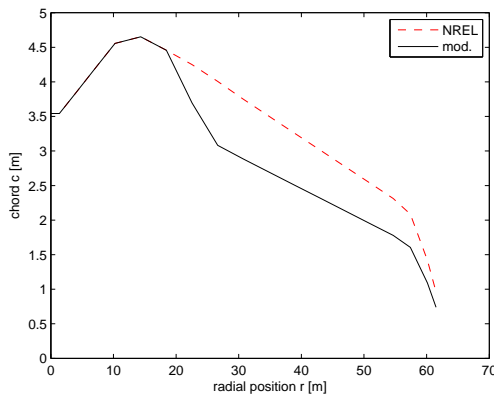
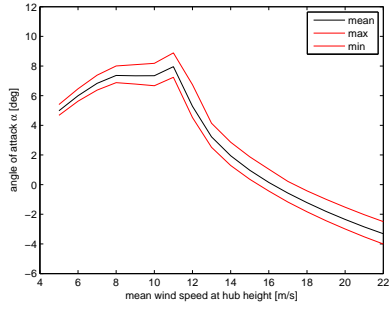


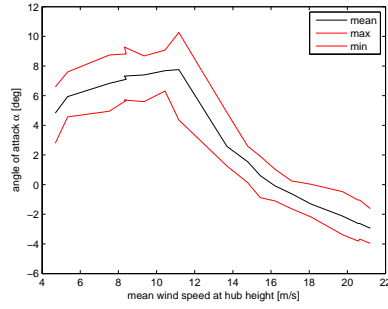
Figure 18. Modification of the chord distribution of the NREL 5MW wind turbine.

coefficient was increased by 30% at the outer part of the blade and the chord was reduced accordingly to achieve the same lift force as on the original blade.

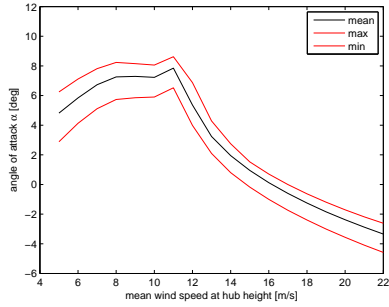
The behaviour of the turbine with modified blades is qualitatively the same as for the NREL 5MW reference turbine, figure 19. The whole figure is simply shifted to higher AoAs. With inflow turbulence the maximum AoA is $\alpha = 10^\circ$. In this case there is still a margin to the stall AoA, but flow separation close to the trailing edge of the airfoil on the suction side is possible. This change illustrates, in principle, how a more aggressive wing design can lead to the blade undergoing transient separation. Figure 20 illustrates in which range of the airfoil polar the blade is operated with the new designed blade. The airfoil is operated above the linear part of the polar, but still below maximum lift angle. For the highest AoAs the region with a steep drag rise is reached. In the original design the blade is operated well within the linear part of the airfoil polar, figure 21. All AoAs are located in the region with the lowest drag. The lift to drag ratio is better than for the modified blade design and flow separation is better suppressed.



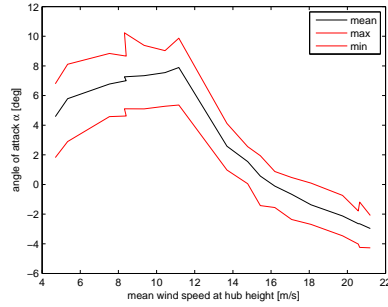
(a) Uniform Inflow, No Turbulence



(b) Uniform Inflow, $T_i=0.2$

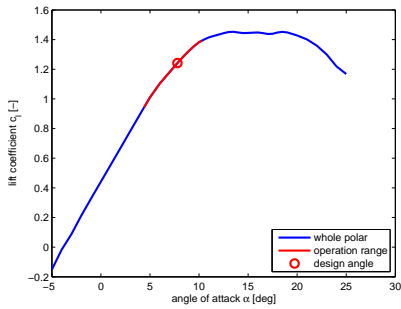


(c) Sheared Inflow $\exp=0.5$, No Turbulence

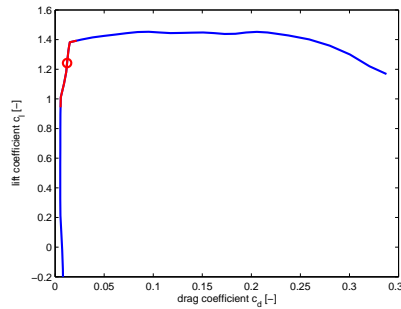


(d) Sheared Inflow $\exp=0.5$, $T_i=0.2$

Figure 19. Amplitude and mean values of the AoA as function of the wind speed for modified blade design.



(a) c_l vs α



(b) c_l vs c_d

Figure 20. Range of operational AoAs in terms of the airfoil polar for modified blade design.

2.3 Surface pressure characteristics of NM80 2.3MW wind turbine (DANAERO)

Note on the presented data: The pressure distribution and the AoA are measured at the radial position $r=31\text{m}$. The surface pressure fluctuations are measured at radial position $r=37\text{m}$ with the microphones. The other systems failed at this position, but CFD computations [7] showed that the AoA at $r=31\text{m}$ and $r=37\text{m}$ is almost identical and the airfoil characteristics are similar. Hence, the pressure distribution should be similar as well.

We chose measurement data from Sept. 1st, 2009 at 10:00 when the turbine experienced extremely sheared inflow conditions. The wind profile measured by a met mast nearby is displayed in figure 22. The measured wind profile is well approxi-

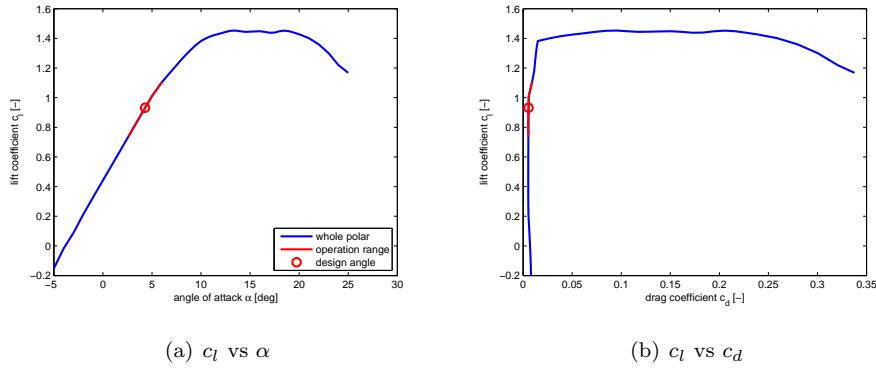


Figure 21. Range of operational AoAs in terms of the airfoil polar for original blade design.

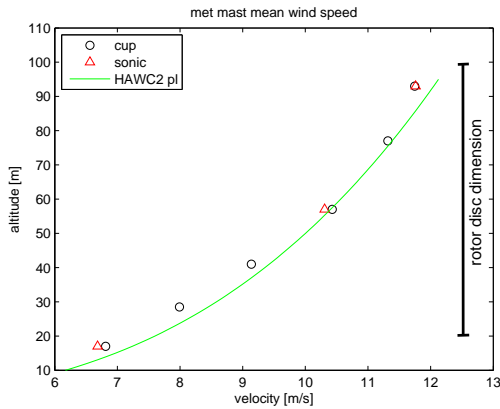


Figure 22. Wind profile measured by a met mast close to the turbine on Sept. 1st, 2009 at 10:00.

mated by a power law function with an exponent of 0.3.

The measurements of the angle of attack at radial position $r = 31\text{m}$ as a function of time reveal a periodic variation, figure 23. The variation is linked to the blade

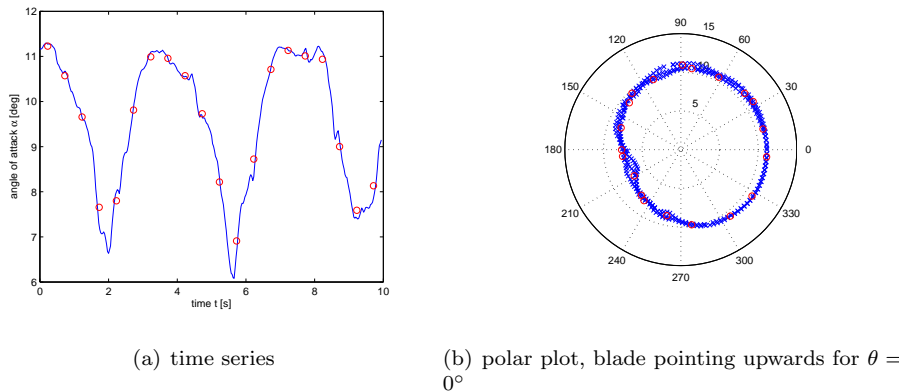


Figure 23. Measured angle of attack at radial position $r = 31\text{m}$. red dots: half second averages.

azimuth position, as can be seen in the polar plot figure 23(b). The maximum AoA is measured for the blade pointing upwards ($\theta = 0^\circ$) and the minimum is reached when the blade pointing down passes the tower ($180^\circ < \theta < 225^\circ$). The variation of the AoA is hence caused by the combined effects of wind shear and tower shadow.

The surface pressure spectrum; the main source of the sound emission, depends on the AoA and the relative velocity of the blade section. The contour plot of

the surface pressure spectrum in the low frequency range ($f < 1000\text{Hz}$) as function of time, figure 24, shows amplitude modulation in the frequency range up to $f < 500\text{Hz}$. High surface pressure levels are associated with high AoAs. The

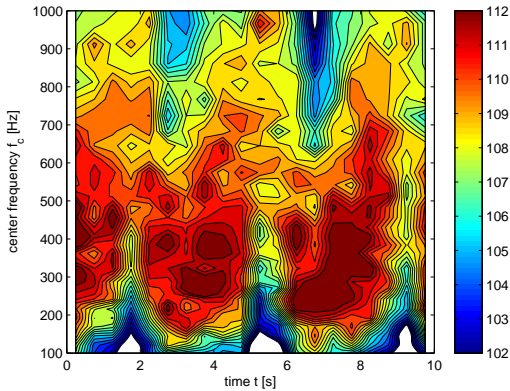


Figure 24. Narrow band spectra of surface pressure measured on Sept. 1st, 2009 at 10:05. PL in dB(1/12th octave).

peak to peak difference of the surface pressure level is about 6dB. In the far field the amplitude modulation will be less pronounced. Unfortunately our data is not sufficient to clarify whether the amplitude modulation of the surface pressure is high enough to cause amplitude modulation in the far field.

To illustrate the correlation between the shape of the surface pressure spectrum and the AoA, we rearranged the data of the 10 second time series by gathering samples within $\pm 0.5^\circ$ of a centre AoA, figure 25. A shift to higher surface pressure

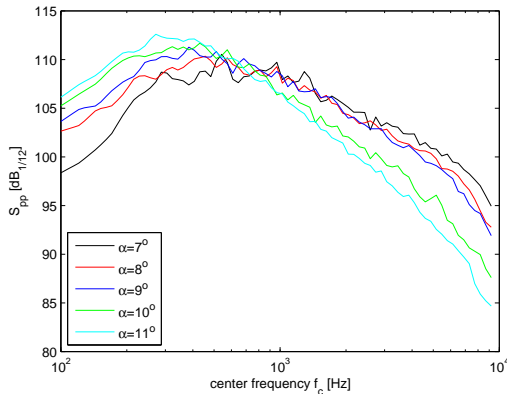
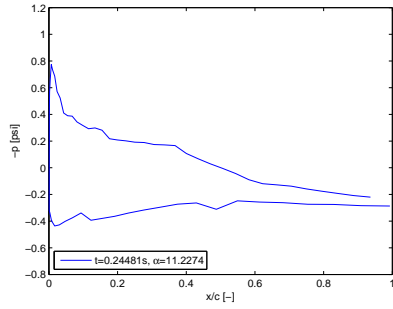
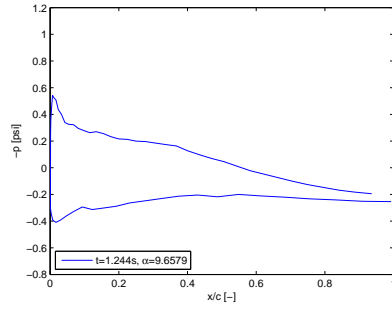


Figure 25. Narrow band spectra of surface pressure binned on angle of attack measured on Sept. 1st, 2009 at 10:05. PL in dB(1/12th octave).

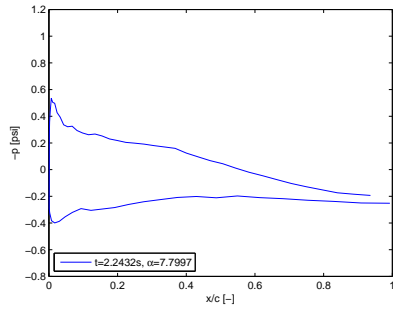
levels in the low frequency range with increasing AoA can be observed. But the shift is very smooth and the rise in level is moderate. The pressure distributions, figure 26, show that even for the highest AoA ($\alpha = 11.2^\circ$) an adverse pressure gradient can be observed at the aft part of the airfoil on the suction side.



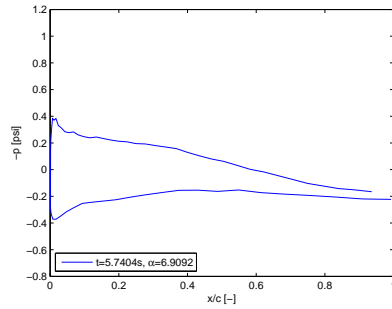
(a) $t = 0.2s, \alpha = 11.2^\circ$



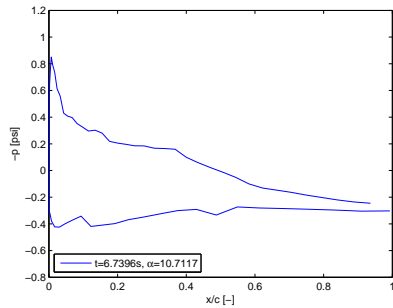
(b) $t = 1.2s, \alpha = 9.7^\circ$



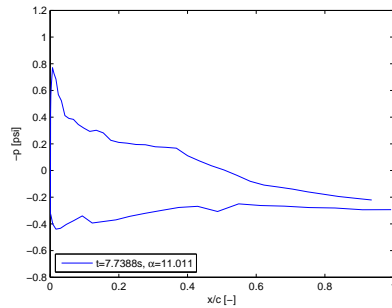
(c) $t = 2.2s, \alpha = 7.8^\circ$



(d) $t = 5.7s, \alpha = 6.9^\circ$



(e) $t = 6.7s, \alpha = 10.7^\circ$



(f) $t = 7.7s, \alpha = 11.0^\circ$

Figure 26. Measured pressure distribution at radial position $r=31m$ on Sept. 1st, 2009 at 10:05 (data is 0.5sec averaged).

Flow separation, characterised by a flat pressure distribution on the aft part of the airfoil on the suction side, does not occur in the whole operational range. At 11:40 a higher wind speed was measured by the met mast, figure 27. The shear is

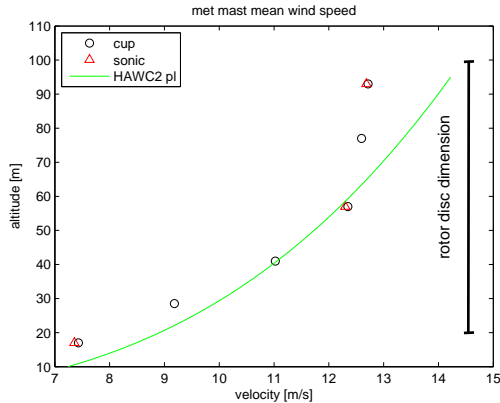
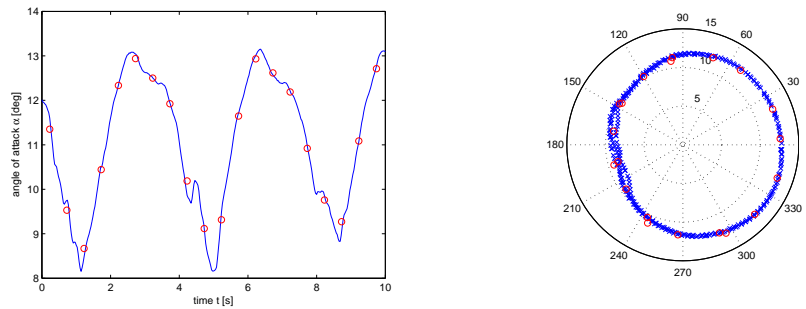


Figure 27. Wind profile measured by a met mast close to the turbine on Sept. 1st, 2009 at 11:40.

very high below the hub height of the wind turbine (60m), but above the inflow profile is nearly constant. The variation of the wind speed over the rotor disc is less than for the previous time series. Due to the higher wind velocity, the wind turbine operates at higher AoAs at radial position $r=31\text{m}$, figure 28. At AoA $\alpha = 13^\circ$ the



(a) time series

(b) polar plot, blade pointing upwards for $\theta = 0^\circ$

Figure 28. Measured angle of attack at radial position $r = 31\text{m}$. red dots: half second averages.

blade is likely to begin to stall. Such a high AoA is reached at azimuth position $\theta = 315^\circ$ to $\theta = 0^\circ$. The corresponding contour plot of the surface pressure spectrum, figure 29, shows a very strong amplitude modulation in the low frequency range ($f < 200\text{Hz}$). The difference in level in the low frequency range in time is up to 14dB. The high levels occur when the AoA is around 13° . The results of binning the data on the AoA and computing the spectrum is shown in figure 30. The energy in the spectrum is shifted gradually from high to low frequencies when going from AoA $\alpha = 8^\circ$ to $\alpha = 12^\circ$. Comparing the spectrum for the AoAs $\alpha = 12^\circ$ and $\alpha = 13^\circ$ one can see a very strong increase in the low frequencies and also an increase in the high frequency range. This abrupt strong increase in the low frequency range is the reason for the amplitude modulation. As the difference in surface pressure level is much higher than for the previous example, it is very likely that the amplitude modulation occurs in the far field as well.

It is also very likely that the high rise of surface pressure level in the low frequency range is associated with the onset of stall. The pressure distributions, figure 31 are not conclusive for high angles of attack. Problems with the pressure measurement system occurred and the calibration of the pressure sensors is only valid in the lin-

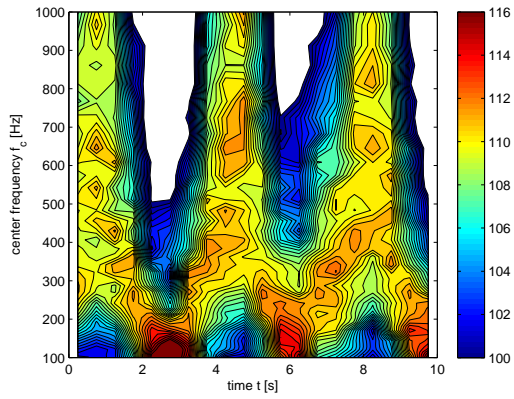


Figure 29. Narrow band spectra of surface pressure at radial position $r=37m$ measured on Sept. 1st, 2009 at 11:48. SPL in dB(1/12th octave).

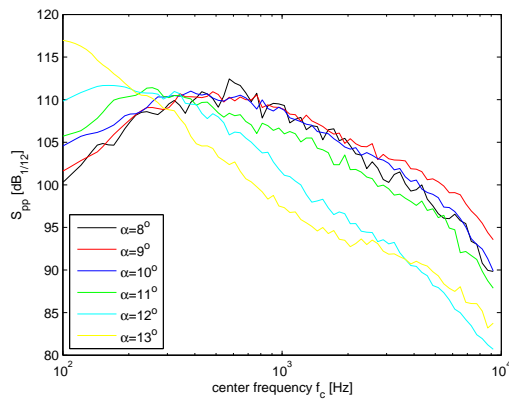
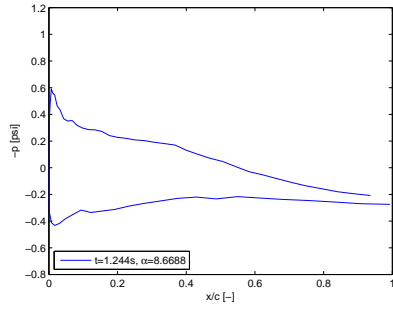
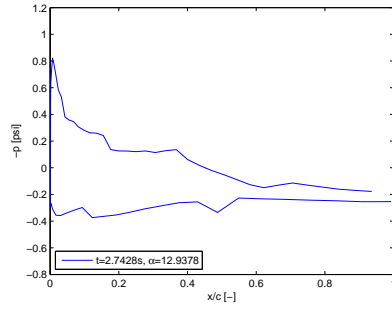


Figure 30. Narrow band spectra of surface pressure binned on angle of attack measured on Sept. 1st, 2009 at 11:48. SPL in dB(1/12th octave).

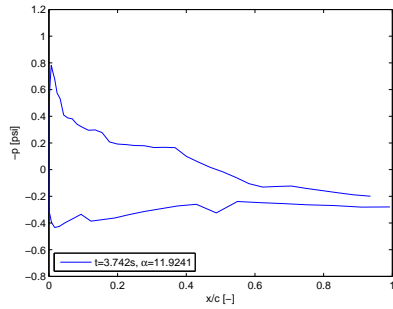
ear range of the airfoil polar. The pressure distributions for AoAs higher than 11° are very irregular as a consequence. One can guess an even pressure distribution on the suction side for $x/c > 0.5$ for both cases with the AoA $\alpha = 12.9^\circ$.



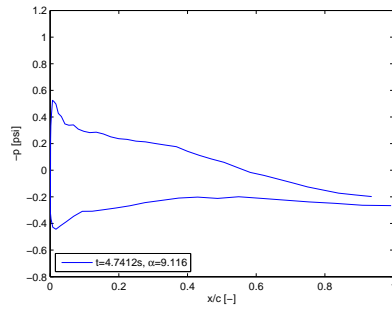
(a) $t = 1.2s, \alpha = 8.7^\circ$



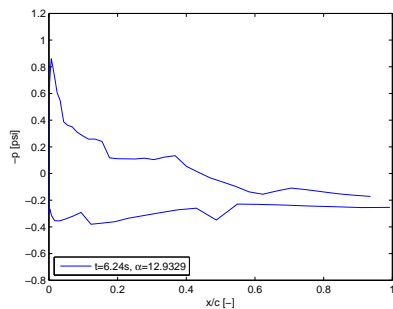
(b) $t = 2.7s, \alpha = 12.9^\circ$



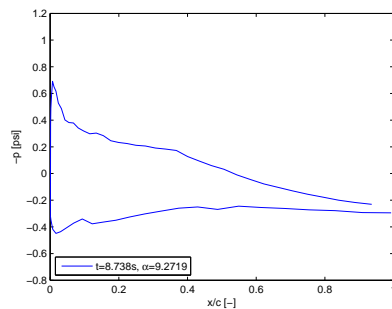
(c) $t = 3.7s, \alpha = 11.9^\circ$



(d) $t = 4.7s, \alpha = 9.1^\circ$



(e) $t = 6.2s, \alpha = 12.9^\circ$



(f) $t = 8.7s, \alpha = 9.3^\circ$

Figure 31. Measured pressure distribution at radial position $r=31m$ on Sept. 1st, 2009 at 11:48 (data is 0.5sec averaged).

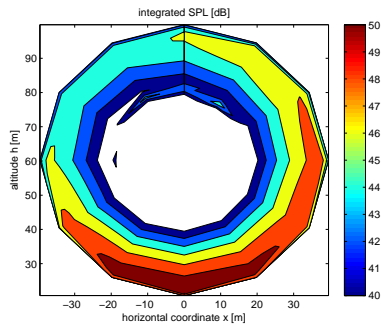
2.4 Aeroacoustic modelling

The computations in this section are carried out with the aeroacoustic model for wind turbine rotors described in the appendix of [8]. A simple BEM model is used to compute the rotor aerodynamics and provide input to the aeroacoustic models. The aeroacoustic part of the code contains engineering models for turbulent inflow (TI) and trailing edge (TE) noise. The programme does not contain a model for stall noise. Hence, it is not very accurate when the blade operates at high angles of attack and it can only be used to describe AM, but not OAM. An error³ existed in the implementation of the TI noise model, which could not be corrected within the scope of this work. The model therefore gives noise levels that are too high - by about a factor 10. However, qualitatively the output seems reasonable. This will be discussed in the following sections.

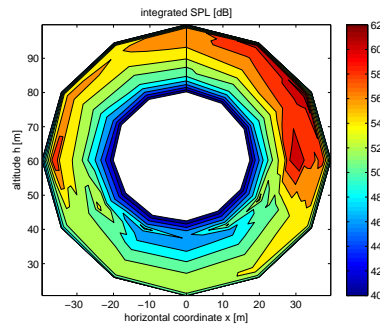
The computations are performed for the turbine geometry of the NM80 turbine. The turbine was run with constant rotational speed of 1.7rad/s (16.2rpm or 0.27Hz). The wind speed at hub height was 10m/s and the turbulence intensity was 10%. The latter is not used in the aerodynamic computations and serves only as input for the TI noise model. The varying parameters of this study were the shear exponent and the pitch setting of the blade. The wind profile was described by an exponential law and we performed computations with a shear exponent of 0.2 (moderate wind shear) and 0.5 (high wind shear). The pitch setting influences the operating point of the blades. The AoA at the blade is shifted to higher values the more we pitch the blade. The computations were performed for a pitch setting of 1.0° and 4.5° corresponding to the experimental conditions described above.

For the computations the blade was discretized in 40 sections and the noise was evaluated at 12 different azimuth positions. We evaluated the noise emitted from each of these discrete positions and received at an observer position located 70m downstream of the rotor at a height of 2m. Figure 32 shows this kind of contour plot for the SPL integrated over all frequencies. This result has to be compared to the SPL computed with only the TE noise model switched on, figure 33, to evaluate the influence of the error in the TI noise model on the overall sound pressure level.

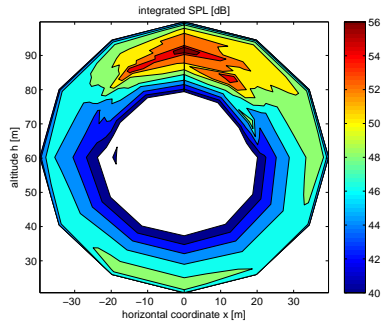
³Communication with Franck Bertagnolio



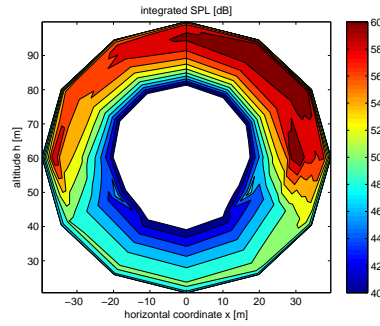
(a) shear exp 0.2, pitch angle 1.0°



(b) shear exp 0.2, pitch angle 4.5°

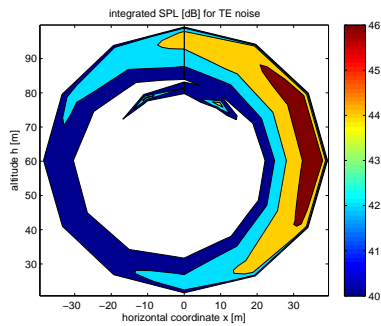


(c) shear exp 0.5, pitch angle 1.0°

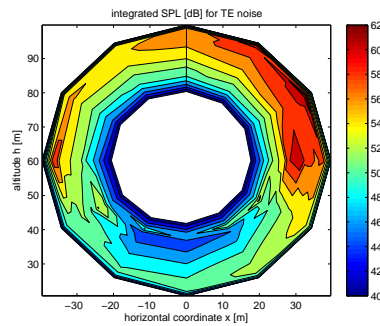


(d) shear exp 0.5, pitch angle 4.5°

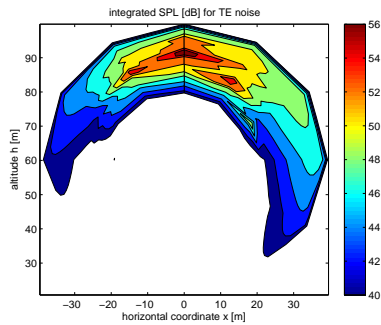
Figure 32. Integrated SPL as a function of the rotor position for an observer 70m downstream of the rotor centre and at 2m height. The rotation of the rotor is clockwise.



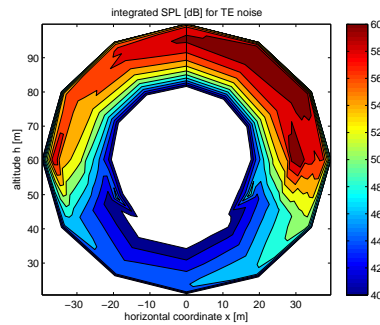
(a) shear exp 0.2, pitch angle 1.0°



(b) shear exp 0.2, pitch angle 4.5°



(c) shear exp 0.5, pitch angle 1.0°



(d) shear exp 0.5, pitch angle 4.5°

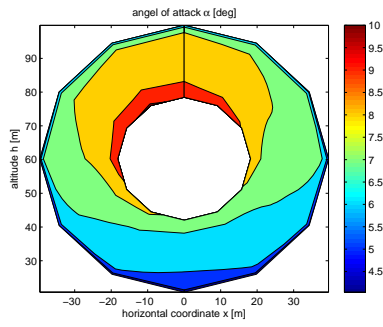
Figure 33. Integrated SPL of TE noise as a function of the rotor position for an observer 70m downstream of the rotor centre and at 2m height. The rotation of the rotor is clockwise.

The comparison of figure 32 and 33 shows that the TE noise mechanism dominates the overall emitted noise in 3 of 4 cases: both cases with high pitch setting and the case with low pitch setting but high shear exponent. With a turbulence intensity of 10% TI noise plays no role in practice, because even with a model overestimating the TI noise source heavily, the SPL generated by the TI noise source is much smaller than the one generated by the TE noise source. For the case with a shear exponent 0.2 and pitch angle 1.0° , the model predicts that the maximum TI noise source is 4dB louder than the maximum TE noise source. But as the TI noise model is assumed to over-predict the SPL by at least 10dB, the TE noise source should be dominant in this case as well. Hence, we assume that the noise source distribution with only the TE noise source modelled is representative for the overall rotor noise source distribution.

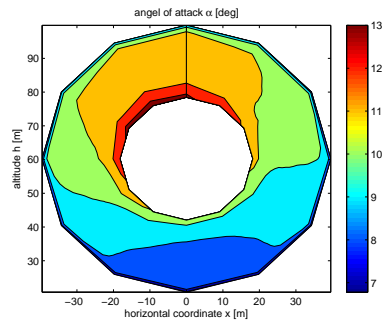
For the high pitch setting ($\theta = 4.5^\circ$), figure 33(b) and 33(d), the noise source distribution is qualitatively similar. The maximum of the SPL is obtained for the blade moving downwards, starting from a 12 o'clock position until the 3 o'clock position. The difference in SPL over one revolution of the blade is about 12dB in the case of shear exponent 0.2 and about 16dB in the case of shear exponent 0.5. For the low pitch setting the overall SPL is significantly reduced compared to the high pitch setting. The noise source distribution is dependent on the shear exponent. With low shear (exponent of 0.2) the highest SPL is emitted when the blade moves from the 1 o'clock position to the 4 o'clock position. The SPL changes only about 6dB over one revolution. With high shear (exponent of 0.5) the highest SPLs are emitted when the blade is at the 12 o'clock position. The difference in SPL over one revolution is more than 16dB. The maximum SPL is 10dB higher for the case with high shear compared to the case with low shear.

TE noise depends mainly on the local flow speed and the angle of attack. The local flow speed to the blade is very similar in all 4 cases, because it is mainly given by the rotational velocity of the blade section and only weakly dependent on the local wind speed. Hence, most of the TE noise is emitted from the outer part of the blade. The angle of attack at the outer part of the blade has its highest values at the 12 o'clock position, figure 34. The maximum TE noise emissions are found at the same position as the maximum AoA at the outer part of the blade, but the apparent noise source strength at the receiver position does not coincide with this in all cases. This is due to the directivity pattern of TE noise. The directivity factor of the noise emission for the specified observer position are shown in figure 35. The directivity is modelled relative to the inflow to the airfoil. Hence it is dependent on the local AoA and we can observe small differences in the directivity factor for the 4 different cases.

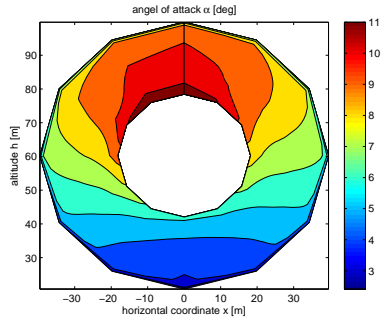
The highest directivity factor are observed for the 3 o'clock to the 5 o'clock position. The position of highest AoAs and highest directivity factor to the observer position are clearly shifted towards each other.



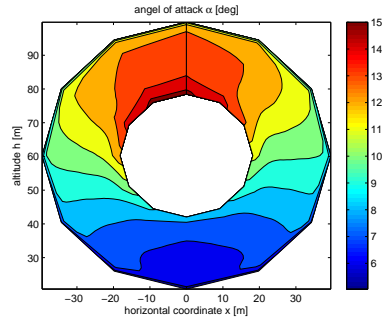
(a) shear exp 0.2, pitch angle 1.0°



(b) shear exp 0.2, pitch angle 4.5°

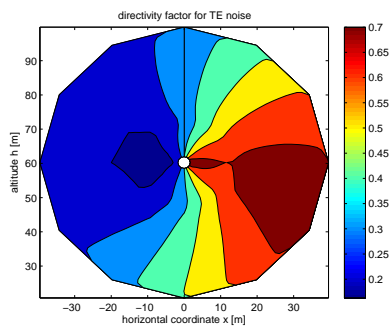


(c) shear exp 0.5, pitch angle 1.0°

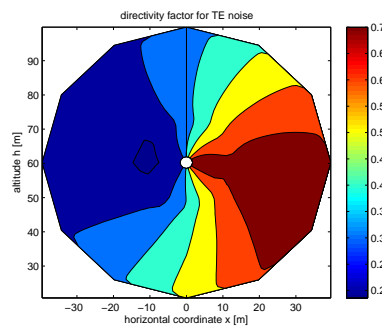


(d) shear exp 0.5, pitch angle 4.5°

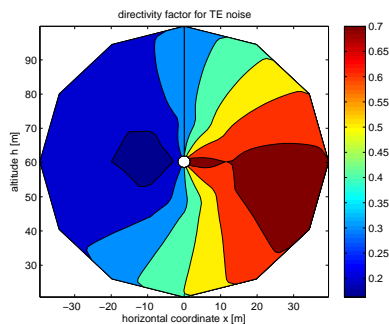
Figure 34. Local AoA at the blade section as a function of the rotor position. The rotation of the rotor is clockwise.



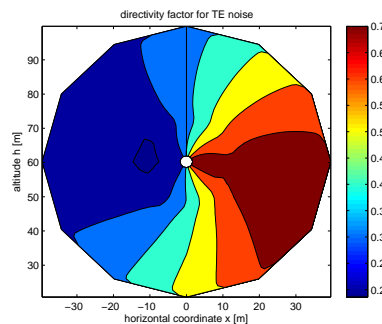
(a) shear exp 0.2, pitch angle 1.0°



(b) shear exp 0.2, pitch angle 4.5°

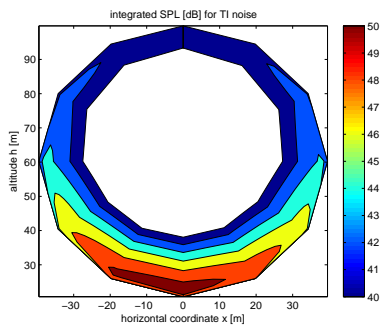


(c) shear exp 0.5, pitch angle 1.0°

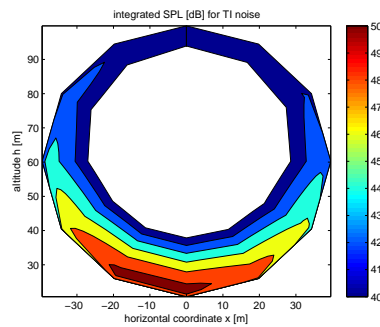


(d) shear exp 0.5, pitch angle 4.5°

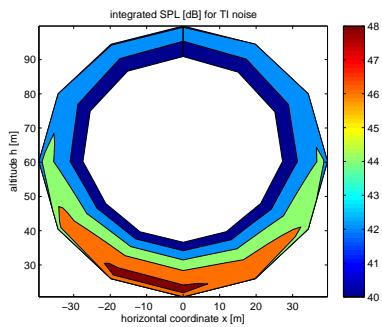
Figure 35. Directivity factor of TE noise as a function of the rotor position for an observer 70m downstream of the rotor centre and at 2m height. The rotation of the rotor is clockwise.



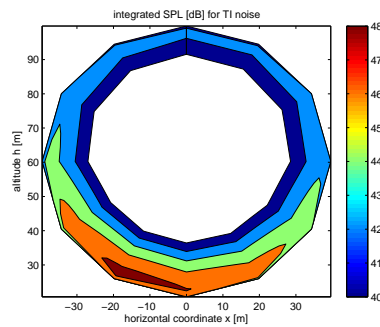
(a) shear exp 0.2, pitch angle 1.0°



(b) shear exp 0.2, pitch angle 4.5°



(c) shear exp 0.5, pitch angle 1.0°



(d) shear exp 0.5, pitch angle 4.5°

Figure 36. Integrated SPL of TI noise as a function of the rotor position for an observer 70m downstream of the rotor centre and at 2m height. The rotation of the rotor is clockwise.

3 WP3: Mitigation Strategies

Both the mean AoA and the AoA variations that have been observed in the results presented in the previous chapters can be decreased using different control strategies. In this chapter, the possibilities of using collective pitch control for decreasing the mean AoA, and the possibilities of using yaw and individual pitch control (IPC) for mitigation of AoA variations are explored.

3.1 Collective Pitch Control

Variable speed turbines are normally operated such that at below rated wind speeds, the pitch is kept at a specified minimum value and the tip speed ratio is kept at its optimal value via regulation of the generator torque. The mean AoA at below rated operation can be decreased if the minimum pitch value is increased. Increasing the minimum pitch will, however, lead to suboptimal operation and decreased power output. The possibilities of decreasing the mean AoA by increasing the minimum pitch angle are investigated by calculating the steady state mean AoA and power production using HawcStab2 (HawcStab2 is an aeroelastic stability simulation tool developed at DTU Wind Energy). In figure 37, the resulting, simulated reductions in mean AoA and power production at different minimum pitch angles are shown. The results have been normalised with the mean AoA and power production at a 0° minimum pitch. From this figure it is evident that it is possible to achieve large reductions of the mean AoA and thus operate further away from the stall region. However, it is also seen that these reductions are obtained at the expense of decreased power production.

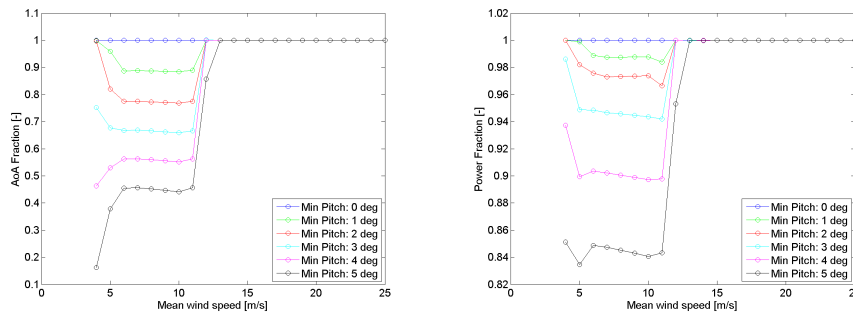


Figure 37. Steady state mean AoA and power production as a function of wind speed when different minimum pitch angles are specified for the variable speed controller. The results are normalised with the mean AoA and power production at a minimum pitch angle of 0°.

3.2 Individual Pitch Control

Usually, IPC is applied at above rated wind speeds for load alleviation, and a variety of individual pitch control schemes have been suggested in the literature. IPC is aimed at alleviating the lift variations that are encountered by the blades during rotation. The lift variations are caused by local inflow variations, such as AoA variations. Therefore, alleviating the azimuthally varying loads using IPC is likely to also lower the AoA variations. To assess the possibilities of mitigating the AoA variations using IPC, a simple IPC is integrated in the turbine controller, and a number of simulations are performed. The IPC that is implemented is similar

to the one described in [9]. The same simulations are performed as those for the modified rotor presented in Chapter 2. The results are shown in Figure 38. The figure shows the steady state AoA variation amplitudes of the IPC controlled turbine relative to the AoA variation amplitudes of the collective pitch controlled turbine.

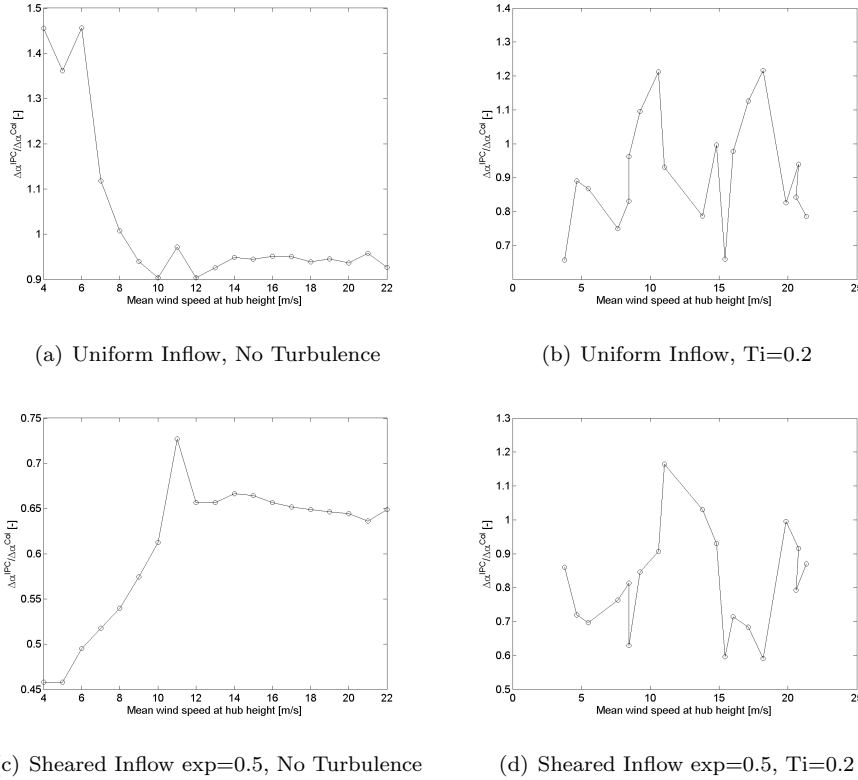
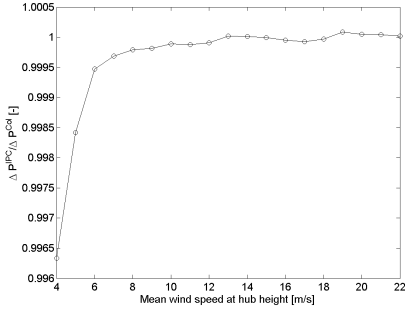


Figure 38. Fraction between the magnitude of the AoA variations for the collective pitch controlled turbine and the individual pitch controlled turbine.

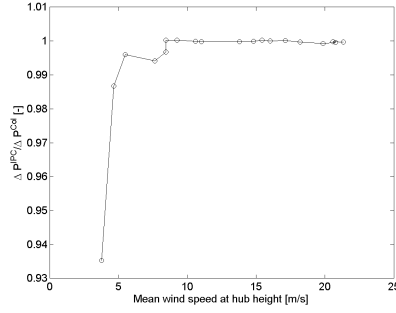
For the uniform inflow, it is seen that the AoA variations are only reduced slightly. This is because the AoA variations are small for a uniform inflow. Furthermore, it is seen that for the uniform inflow, the AoA variations are actually increased by the IPC at wind speeds below 8 m/s. This increase is caused by the IPC that seeks to mitigate blade root bending moment variations. At low wind speeds and uniform inflow the blade root bending moment variations are caused by the gravitational loading on the blades. The gravitationally induced blade loads are mitigated by pitch actuation in phase with the AoA variations, which hereby are increased. For the sheared inflow, it is seen that the AoA variations are significantly lowered at both above and below rated wind speeds. The results for the turbulent simulations are not as consistent as the results for the deterministic simulations. It is therefore possible that the results would be more consistent if the simulations were run with wider wind speed steps allowing longer time and therefore better statistics at each wind speed.

The costs of applying the IPC are increased pitch actuation rates and lowered power output. The power loss is illustrated in Figure 39 that shows the mean power output of the IPC case relative to the non-IPC case. The greatest power loss is observed for low wind speeds (0.35% for uniform inflow and 5.5% for the sheared inflow). At above rated wind speeds there is no power loss due to the IPC. However, in most cases the power loss is below 1%.

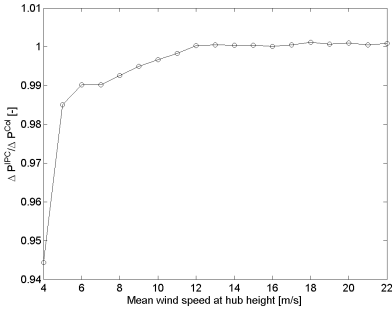
The IPC applied in this study is a standard IPC for load mitigation. It is possible



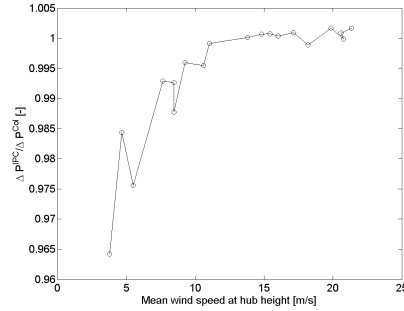
(a) Uniform Inflow, No Turbulence



(b) Uniform Inflow, Ti=0.2



(c) Sheared Inflow exp=0.5, No Turbulence



(d) Sheared Inflow exp=0.5, Ti=0.2

Figure 39. Fraction between the mean power for the collective pitch controlled turbine and individual pitch controlled turbine.

that even larger reductions of the AoA variations could be achieved using on-blade inflow measurements and a controller design for AoA variation mitigation.

3.3 Yaw Control

Yaw control is usually applied to ensure that the rotor is aligned such that the rotor plane is perpendicular to the mean inflow direction. However, yaw control can also be applied for load alleviation [10]. Introducing a certain amount of yaw misalignment in situations with vertical wind shear can also lead to decreased AoA variations. This effect is explored through simulations of the NREL 5MW turbine. Figure 40 shows results from a number of simulations where the yaw misalignment angle is varied at one particular wind speed. It is seen that a yaw misalignment angle can be found that minimizes the range of the AoA variations. Such an optimum yaw misalignment angle can be found for all wind speeds. In Figure 41, the optimum yaw misalignment angles and the resulting range of the steady state AoA variations found from simulations are shown. The ragged appearance of the graphs in Figure 41 is due to the rather rough yaw misalignment angle discretization (5 deg). With a finer resolution a more smooth curve should be obtained.

It is evident that the AoA variations are lowered in the entire wind speed range. However, as seen from Figure 41 significant yaw misalignment is required. Thus, for below rated operation a significant power loss is expected if the AoA variations are mitigated through yaw misalignment. The power loss due to yaw error in uniform inflow can be estimated as:

$$P_{loss} = (1 - \cos(\theta_E))^3 \cdot 100 \quad [\%], \quad (1)$$

where θ_E is the yaw misalignment angle. At well above rated wind speeds yaw

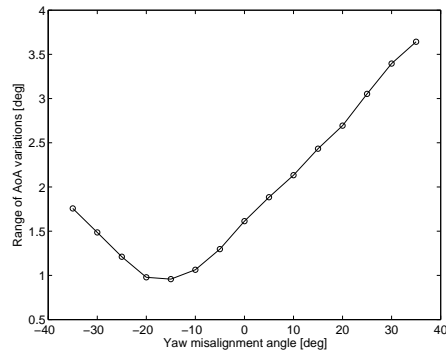


Figure 40. Results of simulations with varying yaw error at a mean wind speed of 8 m/s, no turbulence and a power law wind shear with an exponent of 0.2. A positive yaw misalignment corresponds to an inflow where the wind is approaching the turbine from the right, when seen from the turbine.

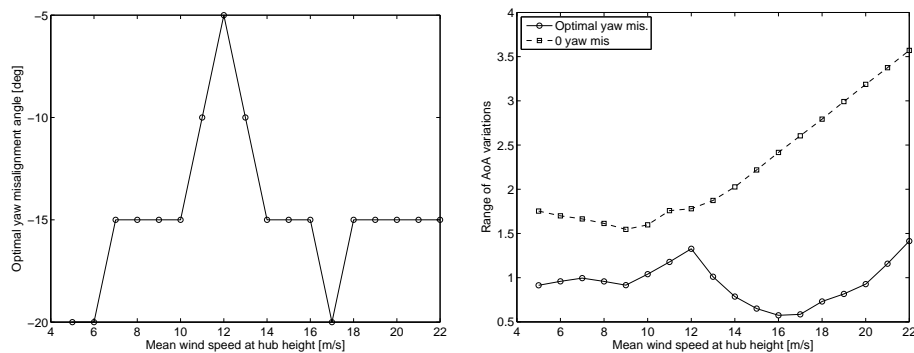


Figure 41. Results of simulations with varying yaw misalignment and mean wind speeds, no turbulence and a power law wind shear with an exponent of 0.2. a) Optimal yaw misalignment angles are identified from the simulations as the yaw misalignment angles that minimizes the AoA variations. b) Range of the simulated AoA steady state variations with 0 zero misalignment and with the optimal yaw misalignment.

misalignment can be introduced without power loss because the power is regulated to the rated value. The power loss introduced by the identified optimal yaw misalignment angle applied in the simulation is shown in Figure 42. It is seen that the power is actually increased at below rated wind speeds when the optimal yaw misalignment angle is applied. Recalling Equation (1) it is surprising that the power is not decreased at below rated wind speeds when the optimal yaw misalignment is applied. However, the increased power might be explained by the asymmetric inflow to the turbine. This phenomena should be investigated further.

The results related to yaw misalignment are all from simulations in deterministic inflow with no turbulence. Thus, the results only indicates the potential of using yaw misalignment for mitigating AoA variations. Simulations in turbulent inflow remain to be performed.

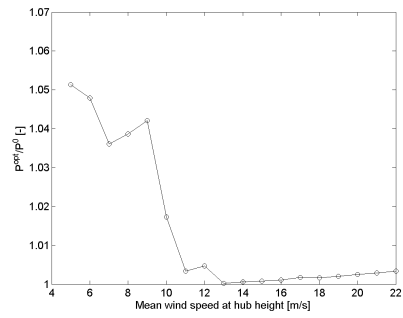


Figure 42. Simulation results. Fraction between the mean power with the optimal yaw misalignment applied and the mean power at 0° yaw misalignment.

4 WP4: Effect of Stall on Noise Emission

The data presented in this section was obtained by measurements made in Virginia Tech University's wind tunnel in 2011. All details about the experiment are found in [11].

4.1 Airfoil aerodynamics

We tested two different airfoils in the anechoic wind tunnel of Virginia Tech University: the NACA64-618 airfoil and a trailing edge noise optimised airfoil based on the previous one, called NACA64-618t. Those two airfoil differ significantly in the stall behaviour. The C_l vs α -polar, figure 43, show that the NACA64-618t has a very abrupt and hard stall behavior characterised by a sudden drop in lift while the NACA64-618 stalls gradually. This difference is advantageous for the

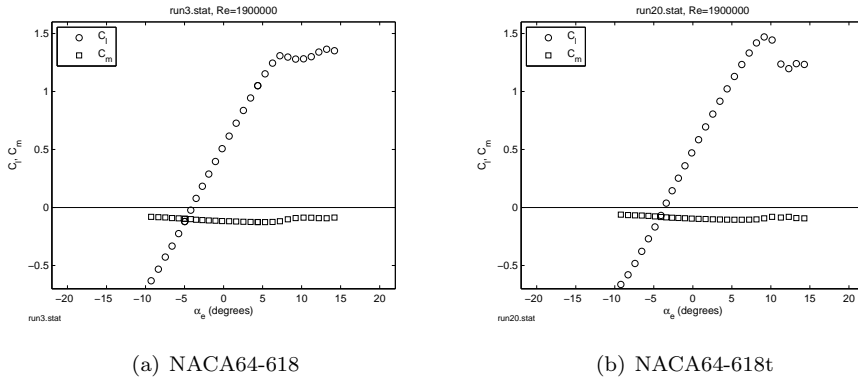


Figure 43. C_l vs α -polar of the two airfoils measured in the Virginia Tech wind tunnel at Reynolds number $1.9 \cdot 10^6$. The AoA is corrected for wall and blockage effects.

present analysis, because we can study the effect of stall on the noise emission for two aerodynamically completely different airfoils.

We use the following terminology for this report to describe the different states of the airfoil flow:

- Pre stall: AoA range with linear increase of the lift coefficient before maximum lift is reached. In this region the flow is attached to the airfoil.
- Post stall: typically the first AoA measured beyond maximum lift. Separation of the flow from the airfoil starts to occur and covers a small part of the chord length.
- Deep stall: AoAs far beyond the maximum lift AoA. The flow is separated over large parts of the chord length.

4.2 Far field Sound and Surface Pressure for High AoAs

The acoustic array measurement technique is limited to frequencies higher than 500Hz. Due to background noise in the wind tunnel, the measurements are often limited to even higher frequencies. This frequency is determined by looking into the acoustic map to check if the trailing edge is visible as a noise source. The limit

is typically about 700Hz. The important frequency content of sound emission from stalled airfoils in this configuration is most likely in the range below 500Hz. We can only measure the surface pressure fluctuations in the low frequency range. The model to convert surface pressure fluctuations into far field sound is only valid for attached flow. Hence, we need to analyse the far field sound in stalled flow conditions in the measurable frequency range together with the surface pressure fluctuations. From the result of this analysis we can draw conclusions about the sound emission of stalled airfoils in the high frequency range and try to link qualitatively the surface pressure fluctuations with the far field sound. Then we can try and transfer the results to the low frequency range by means of measured surface pressure fluctuations.

The far field sound pressure spectra of the two airfoils for a pre, post and deep stall AoA are shown in figure 44. Both airfoils show a strong increase in the overall noise

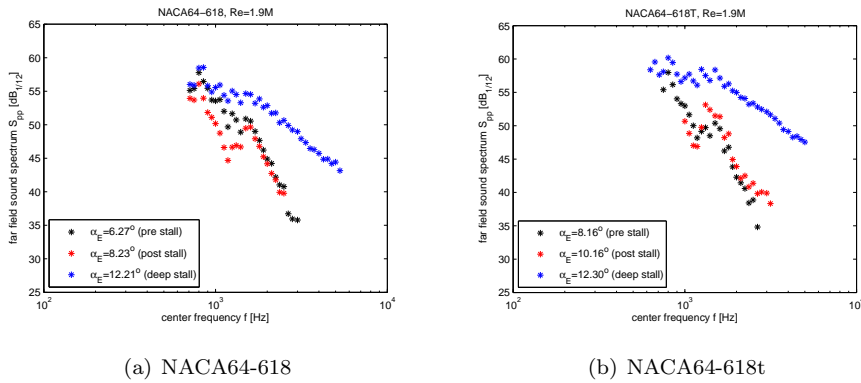


Figure 44. Far field sound pressure spectra for several AoAs of the two airfoils measured in the Virginia Tech wind tunnel at Reynolds number $1.9 \cdot 10^6$.

level when the airfoil is in deep stall ($\alpha > 12^\circ$). However, in the mid frequency range the levels are very similar and due to the limitation of the measurements we can draw no conclusion for the low frequency range. Comparing the two airfoils, the NACA64-618t airfoil in deep stall is more noisy than the NACA64-618 airfoil. There is a link to the aerodynamic stall properties.

We find a big difference between the two airfoils when looking at AoAs in the stall region, figure 45. The noise level increases gradually for the NACA64-618 airfoil

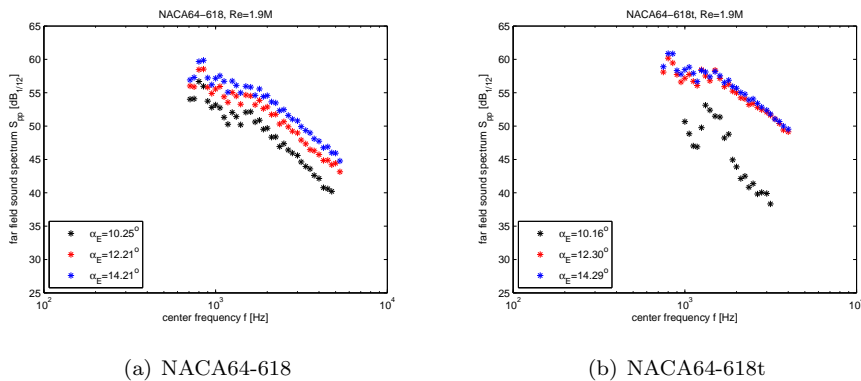


Figure 45. Far field sound pressure spectra for several AoAs in stall of the two airfoils measured in the Virginia Tech wind tunnel at Reynolds number $1.9 \cdot 10^6$.

with the AoA. For the NACA64-618t the far field sound pressure level jumps together with the jump in lift. An increase in sound pressure level of about 7dB for a change in the AoA of only 2.1° is observed. The jump in lift is observed

within a change in AoA of 1° . The sound pressure level is only measured every 2° . As we expect a direct link between the two phenomena, we also expect the gradient of the SPL change to be steeper. This can be checked by refining the AoAs in the measurement matrix.

The effects of stall on airfoil noise in the low frequency range have to be estimated qualitatively by means of the surface pressure. Even though the far field noise models are not valid in stall, we expect the far field noise level to follow the surface pressure level. The surface pressure spectra at chord position $x/c = 0.975$ for the same AoAs as the far field sound in figure 44 are displayed in figure 46. Note

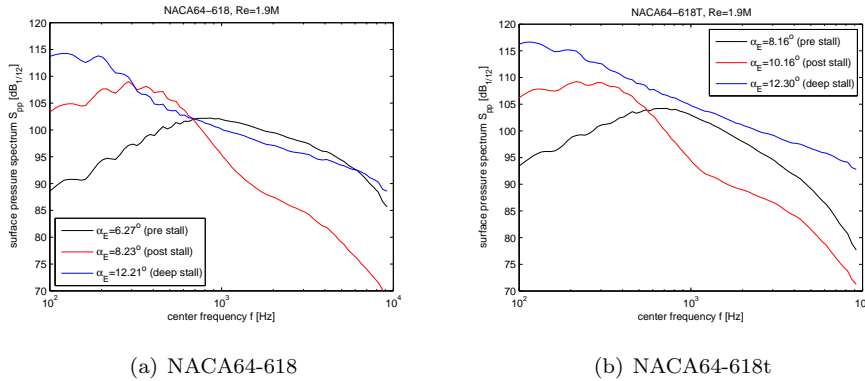


Figure 46. Surface pressure spectra at chord position $x/c = 0.975$ for several AoAs of the two airfoils measured in the Virginia Tech wind tunnel at Reynolds number $1.9 \cdot 10^6$.

that the wavy shape of the spectra in the low frequency range ($f < 500\text{Hz}$) is due to wave reflections in the tubing system of the surface pressure microphones and the imperfect compensation for temperature shift in the calibration function. The surface pressure level (PL) for pre stall conditions is significantly higher than for post stall conditions in the mid frequency range ($f > 1000\text{Hz}$). This is not reflected in the far field sound pressure spectra, figure 44. For the NACA64-618 the far field SPL is slightly higher for pre stall conditions than for post stall conditions, but the difference is by far less than the difference in the surface PL. For the NACA64-618t the far field SPL for the pre and post stall conditions are almost identical. In deep stall the far field sound and the surface PL of the NACA64-618t are the highest in the mid frequency range. The far field SPL of the NACA64-618 is the highest in deep stall, but the surface PL is lower than for pre stall conditions. We conclude that the relationship between far field SPL and surface PL in pre and post stall conditions are different. But qualitative estimations of the far field SPL based on surface PL can be done with care.

We then analysed the surface pressure spectra and used the previous findings to conclude about the far field sound in the low frequency range. The surface pressure spectra show clearly a shift of the energy to low frequencies ($f < 600\text{Hz}$) when going from pre to post stall for both airfoils. The difference of the level is more than 10dB at a frequency of 200Hz. Such a large difference must be reflected in the far field SPL. When going from post to deep stall the overall surface PL increases. The increase of the overall surface PL is larger for the NACA64-618t airfoil than for the NACA64-618. The increase in surface PL at a frequency of 200Hz is again in the order of 10dB. If an airfoil operates in or close to the stall region, strong changes in the surface PL in the low frequency range go hand in hand with relatively small changes in the AoA. Hence, we also expect the far field SPL in the low frequency range to change significantly with very small changes in AoA. This mechanism can lead to amplitude modulation in the far field.

4.3 Far field Sound Modelling for high AoA in Pre Stall

With the trailing edge noise models described in [11] one can gain more direct information about the far field sound in the low frequency range. However, the model is restricted to AoAs in pre stall conditions.

In [11] two different models used to estimate the far field SPL by means of the measured surface pressure frequency wave number spectrum were investigated: 1) the model of Howe [12] and 2) Amiet’s model with Roger’s extensions [13]. In the high frequency range both models give almost identical results, but in the low frequency range significant differences can be observed. Amiet’s model with Roger’s extensions takes the finite chord length of the airfoil into account and models the back-scattering effect from the leading edge. Those effects are important in the low frequency range. Hence, we use only this model here.

The measured and predicted far field SPLs of the NACA64-618t airfoil for various pre stall AoAs are depicted in figure 47. Predictions and Measurements are in very

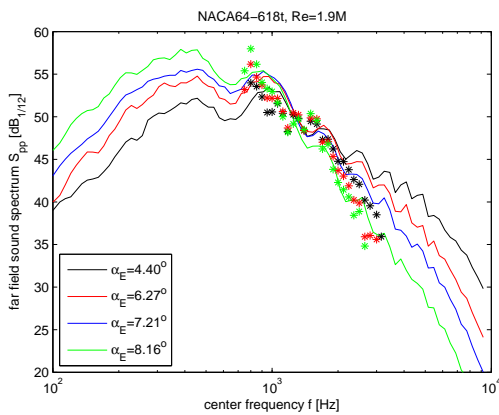


Figure 47. Far field SPL for AoAs in pre stall condition for the NACA64-618t at Reynolds number $1.9 \cdot 10^6$. Solid lines: Amiet Model, stars: microphone array measurement.

good agreement in the mid frequency range ($800\text{Hz} < f < 2000\text{Hz}$). For higher frequencies they start to deviate. The model predicts much larger differences in SPL than the measurements show. The model also predicts very big differences in SPL along with only small changes in AoA, especially for high AoAs. The difference of SPL at 200Hz when going from $\alpha = 7.21^\circ$ to $\alpha = 8.16^\circ$ is 2.8dB. Such a difference can cause OAM. But this result has to be considered with care, because it is only based on model predictions without a direct measurement.

4.4 Conclusions

The analysis of the FF sound data of the Virginia Tech experiment identifies 3 possible causes for OAM:

1. An alteration in AoA causing the flow condition to alternate from pre to post stall. In this case a large difference in SPL was observed on both airfoils. It is a condition which should be avoided in every case.
2. For airfoils with very abrupt stall behaviour like the NACA64-618t we found a large jump in SPL when changing AoA by less than 2° in the stall region. It is probably caused by a very sudden change from partial to full separation of the flow.
3. The model of Amiet with Roger’s extensions predicts large differences of FF SPL in the low frequency range for relatively small changes in AoA. This result has to be handled with care, because there are no direct measurements

to support this observation so far. But if the model results reflect reality, OAM without stalled flow conditions could be possible.

References

- [1] I. Antoniou, R. Wagner, S. M. Pedersen, U. Paulsen, H. A. Madsen, H. E. Jørgensen, K. Thomsen, P. Enevoldsen, and L. Thesbjerg. Influence of wind characteristics on turbine performance. In *Proc. of the EWEC2007*, Milan, IT, 2007.
- [2] H. A. Madsen and A. Fischer. Wind shear and turbulence characteristics from inflow measurements on the rotating blade of a wind turbine rotor. In *Proc. of the EWEC2009*, Marseilles, FR, 2009.
- [3] H. A. Madsen, C. Bak, U. S. Paulsen, M. Gaunaa, P. Fuglsang, J. Romblad, N. A. Olesen, P. Enevoldsen, J. Laursen, and L. Jensen. The DAN-AERO MW Experiments: Final report. Tech. Rep. Risø-R-1726(EN), Risø-DTU, Roskilde, Denmark, September 2010.
- [4] H. A. Madsen, V. Riziotis, F. Zahle, M. O. L. Hansen, H. Snel, F. Grasso, T. J. Larsen, E. Politis, and F. Rasmussen. Blade element momentum modeling of inflow with shear in comparison with advanced model results. *J. of Wind Energy*, 2011. Published online in Wiley Online Library (wileyonlinelibrary.com). DOI: 10.1002/we.493.
- [5] J. Jonkman, S. Butterfield, W. Musial, and G. Scott. Definition of a 5-MW Reference Wind Turbine for Offshore System Development. Tech. Rep. NREL/TP-500-38060, National Renewable Energy Laboratory, Golden, Colorado, USA, February 2009.
- [6] J. Mann. The spatial structure of neutral atmospheric surface-layer turbulence. *J. of Fluid Mech.*, 273:141–168, 1994.
- [7] N. N. Sørensen, N. Troldborg, J. Johansen, J. Madsen, and P. E. Rethore. Comparison of CFD rotor simulations with DANAERO measurements. In *DANAERO MW: Final Report*, Roskilde, Denmark, April 2013.
- [8] J. Bass, H. A. Madsen, F. Bertagnolio, and A. Fischer. Description of contract work for renewable on mechanisms of am and oam, 2013.
- [9] E. A. Bossanyi. Individual blade pitch control for load reduction. *Wind Energy*, 6(2):119–128, 2003.
- [10] Knud A. Kragh and Morten H. Hansen. Load alleviation of wind turbines by yaw misalignment. *Wind Energy*, pages n/a–n/a, 2013.
- [11] A. Fischer. *Experimental characterization of airfoil boundary layers for improvement of aeroacoustic and aerodynamic modeling*. PhD thesis, DTU Technical University of Denmark, Roskilde, Denmark, November 2011.
- [12] M. S. Howe. A Review of the Theory of Trailing Edge Noise. *J. Sound Vib.*, 61(3):437–465, 1978.
- [13] M. Roger and S. Moreau. Back-scattering correction and further extensions of Amiet’s trailing-edge noise model. Part 1: theory. *J. Sound Vib.*, 286:477–506, 2005.

A Turbines used in the investigation and influence of turbine size

A.1 The 5MW NREL reference turbine

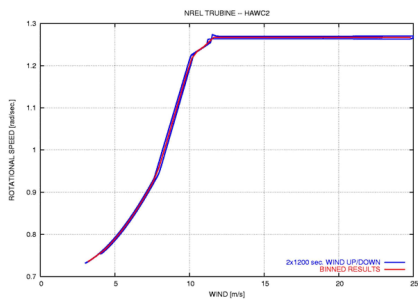
Data on blade planform (chord and twist as a function of radius) and operational conditions (e.g. rpm and pitch as a function of wind speed) are generally not made publicly available by manufactures. However, in the research community there is a need to have such data in order to test models, to study wind turbine aerodynamics and aeroelasticity and in general to carry out research on wind turbine rotors. This led to the definition of the 5MW reference wind turbine by National Renewable Energy Laboratory (NREL) in the US [5]. We cite the following from the executive summary of [5]:

”To support concept studies aimed at assessing offshore wind technology, we developed the specifications of a representative utility-scale multimegawatt turbine now known as the NREL offshore 5-MW baseline wind turbine. This wind turbine is a conventional three-bladed upwind variable-speed variable blade-pitch-to-feather-controlled turbine. To create the model, we obtained some broad design information from the published documents of turbine manufacturers, with a heavy emphasis on the REpower 5M machine. Because detailed data was unavailable, however, we also used the publicly available properties from the conceptual models in the WindPACT, RECOFF, and DOWEC projects. We then created a composite from these data, extracting the best available and most representative specifications. This report documents the specifications of the NREL offshore 5-MW baseline wind turbine including the aerodynamic, structural, and control-system properties and the rationale behind its development. The model has been, and will likely continue to be, used as a reference by research teams throughout the world to standardise baseline offshore wind turbine specifications and to quantify the benefits of advanced land- and sea-based wind energy technologies.”

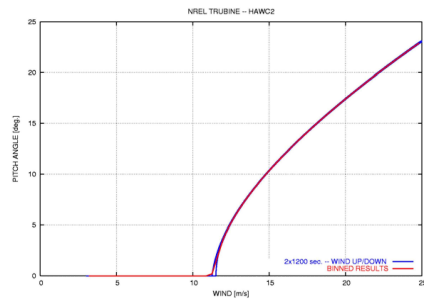
So the reference turbine is close to the REpower 5M machine. The design data in [5] allow detailed aerodynamic and aeroelastic simulations and is thus well suited to be used in a study like the present. However, as discussed in section 2.2 the turbine operates at an inflow angle range that is in a safe distance from stall and some of the commercial turbines have a more slender blade design causing the operational point on the lift curve to be closer to stall. We demonstrated this change in the design by reducing the chord, figure 18, and showed how this had the effect of pushing the operational point closer to stall, figure 20. Finally, the operational characteristics for the turbine and the power curve are shown in figures 48 and 49, respectively.

A.2 The NM80 turbine

The other turbine involved in the work is the NM80 turbine where we carried out the detailed inflow measurements and surface microphone measurements in the DANAERO MW project. The measurements from this machine were introduced in order to show how the surface pressure spectra changes during operation in extreme shear, where the turbine was forced to approach stall by using a constant speed of operation and by running the turbine at extreme negative pitch. Both the constant rpm and the negative pitch are far from normal operation. In addition, while this turbine is a standard variable speed, pitch-regulated turbine but we were unable to show the turbine characteristics in its normal mode for reasons of confidentiality.



(a) rotational speed



(b) pitch angle

Figure 48. Variation of rotational speed and pitch as a function of wind speed.

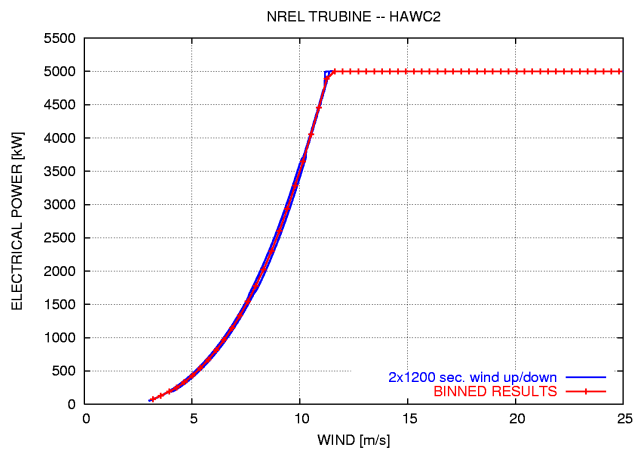


Figure 49. Computed power curve as a function of wind speed for the 5MW reference wind turbine.

B Difference between angle of attack AoA and inflow angle IA

The angle AoA for an airfoil section is the angle between the chord of an airfoil section and the direction of the incoming flow described by the streamlines, figure 50. However, as seen on figure 50 the streamlines bend when they approach the

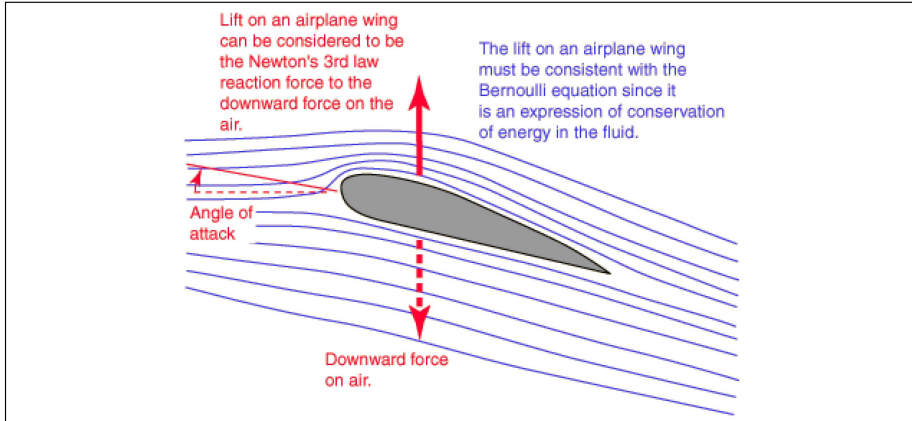


Figure 50. Illustration showing definition of AoA and how the streamlines bend when they approach the airfoil. From <http://hyperphysics.phy-astr.gsu.edu/hbase/fluids/angatt.html>

airfoil; upwards on the upper side and downwards on the lower side. When measuring the inflow on the blade of a wind turbine rotor with e.g. a five hole pitot tube, figure 51, it will often be made rather close to the airfoil section. We then measure a flow direction called inflow angle IA that is influenced by the airfoil section itself. If it is along the red solid line close to the airfoil in figure 50 we will measure a bigger angle (IA) than the AoA. Based on simulations of the flowfield

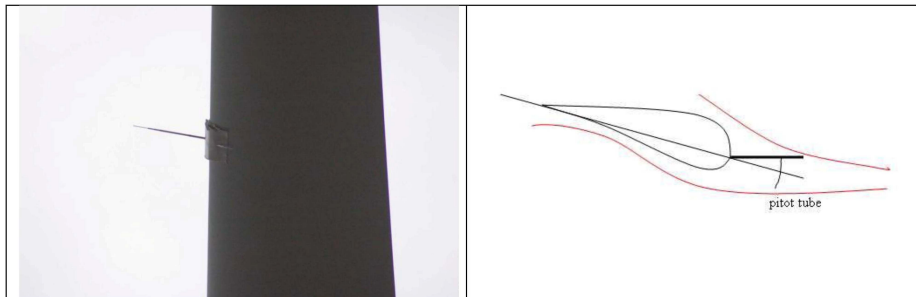


Figure 51. To the left is seen the five hole pitot tube mounted on the leading edge of the blade of the 3.6MW Siemens wind turbine at the Høvsøre test site in Denmark. The pitot tube is about 1m long and measures the direction and magnitude of the incoming flow.

around the rotor blade it is possible to derive a calibration equation to convert from AoA to IA for the specific blade design and pitot tube.

In the aerodynamic and aeroelastic simulations the AoA is computed and in WP1 we wanted to see if we would get the same simulated IA for the specific wind shear as measured. Therefore we applied the conversion of simulated AoA to IA, figure

Technical University of Denmark
DTU Vindenergi

info@vindenergi.dtu.dk
www.vindenergi.dtu.dk